Modelling of STEFF NaI detectors using the MCBEND Monte Carlo code.

A thesis submitted to the University of Manchester for the degree of Masters of Science by research in nuclear physics in the Faculty of Engineering and Physical Sciences

2013

James Cubiss

School of Physics and Astronomy

Table of Contents

List of Figures

Abstract

The MCBEND program provided by the ANSWERS group at AMEC is a general purpose radiation transport code for electron, neutron and gamma-ray transportation, within systems in a sub-critical state. The program was used to model the response of a NaI, cylindrical detector of dimensions 51 mm diameter and 51 mm depth, to gamma ray energies of 1.173 MeV and 1.332 MeV produced by the decay of a ^{60}Co source. Two further programs were then used, one to produce a broadening on the data in order to replicate the effects of the energy resolution of the detector and another to generate a sum peak such as the one observed in the experimental results.

Comparisons were made between the MCBEND, MCNP and GEANT4 Monte Carlo codes. This was done by modelling the response of a STEFF NaI detector to the decay of a ^{60}Co source. A simulation was also run for a gamma-ray of energy 4 MeV for each code in order to see how they dealt with high energy gamma-ray calculations.

A reference library was created using MCBEND for gamma-ray energies ranging from 50 keV to 1.5 MeV in 50 keV steps. Using published intensities and energies, a ^{152}Eu spectrum was modelled using MCBEND and compared to an experimentally measured one.

Declaration

No portion of the work referred to in the thesis has been submitted in support of an application for another degree or qualification of this or any other university or other institute of learning.

Copyright Statement

i. The author of this thesis (including any appendices and/or schedules to this thesis) owns any copyright in it (the "Copyright") and s/he has given The University of Manchester the right to use such Copyright, including for administrative purposes.

ii. Copies of this thesis, either in full or in extracts and whether in hard or electronic copy, may be made **only** in accordance with the Copyright, Designs and Patents Act 1988 (as amended) and regulations issued under it or, where appropriate, in accordance with licensing agreements which the University has from time to time. This page must form part of any such copies made.

iii. The ownership of certain Copyright, patents, designs, trade marks and other intellectual property (the "Intellectual Property") and any reproductions of copyright works in the thesis, for example graphs and tables ("Reproductions"), which may be described in this thesis, may not be owned by the author and may be owned by third parties. Such Intellectual Property and Reproductions cannot and must not be made available for use without the prior written permission of the owner(s) of the relevant Intellectual Property and/or Reproductions.

iv. Further information on the conditions under which disclosure, publication and commercialisation of this thesis, the Copyright and any Intellectual Property and/or Reproductions described in it may take place is available in the University IP Policy (see http://documents.manchester.ac.uk/DocuInfo.aspx?DocID=487), in any relevant Thesis restriction declarations deposited in the University Library, The University Library's regulations (see http://www.manchester.ac.uk/library/aboutus/regulations) and in The University's policy on Presentation of Theses.

Acknowledgements

Throughout my studies over the past year there have been several people who have been of great help and deserve to be thanked. Without them, I would not have been able to take part in the following study.

First and foremost I would like to thank my mother and father for their generosity and their constant support and patience throughout the duration of my studies. Without them, none of the following would have been possible and I would like to express my up most gratitude for their many contributions.

Secondly I would like to thank my project supervisor Jon Billowes for his guidance and expertise throughout the duration of the year as well as his support in my application for further study at a doctoral level. Thank you for accepting me on to the MSc course and introducing me to the world of academic research.

I would also like to thank Tim Ware for his patience and supervision whilst I got to grips with the MCBEND and MCNP codes, his provision of the Resbroad code used for broadening of line spectra in the following work and also his support in my applications for further studies.

I would also like to thank Andrew Pollitt for providing the results for the GEANT4 simulations used in the following investigation as well as his advice for the future.

Thank you to Jo Dare for his aid and supervision in the lab at the beginning of the year.

Finally I would like to thank the rest of my family and my friends in their support and faith in my studies over the year and for providing me with ample entertainment outside of my work environments at the University or at the restaurant.

1. Introduction

The Spectrometer for Exotic Fission Fragments (STEFF), shown in Figure 1.1, is a 2-velocity, 2-energy detector. It is designed to provide a better understanding of energy distributions and multiplicity of fission fragments resulting from neutron induced fission [1].

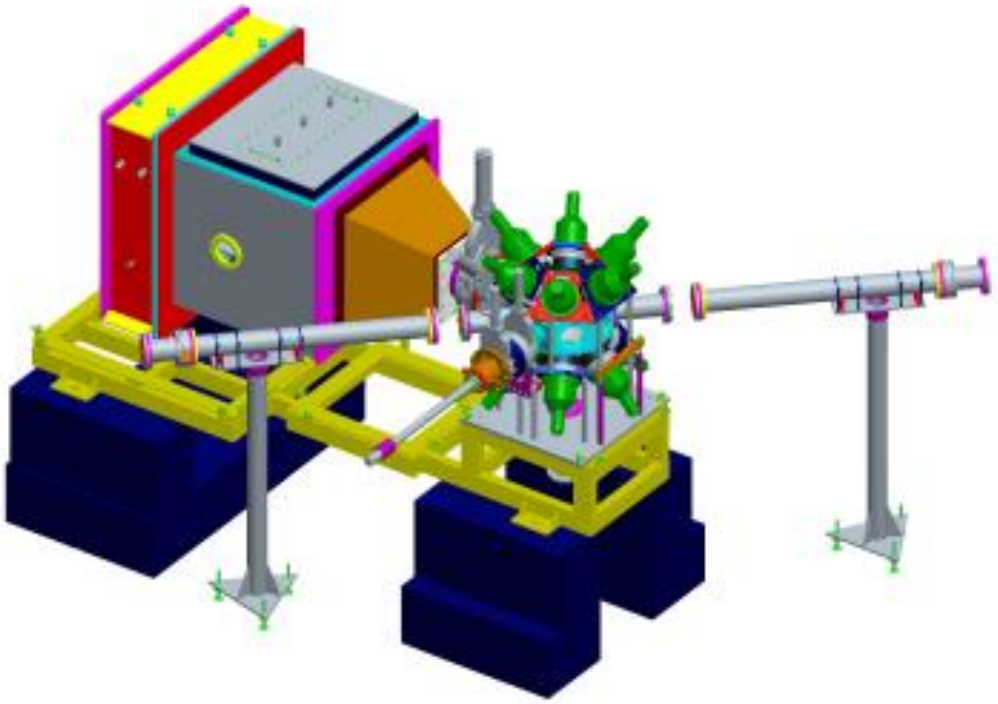

Figure 1.1 - Three dimensional computer generated image of STEFF [2].

The STEFF detector was built by the University of Manchester and has been used in experimentation at the Institut Laue-Langevin (ILL) facility in Grenoble since 2011. Future plans involve moving STEFF to the Grand Accélérateur National d'Ions Lourds (GANIL) facility in Caen.

1.1 The STEFF project

Motivation for the STEFF project comes from within the nuclear energy industry. Prompt gamma ray radiation from the fission of ^{235}U causes heating within nuclear reactors, the amount of heating caused by these gamma-rays has large discrepancies of up to 15%. The STEFF project aims to produce high accuracy

data that will allow for more precise calculations with regards to gamma heating and so allowing for improvements to nuclear reactor design.

Figure 1.2 is a detailed, cross-sectional diagram of the apparatus that is used in STEFF. This includes an array of twelve NaI detectors placed around the central fissile source position. A schematic of the detectors used is shown in Figure 1.3. This array of detectors gives an absolute photopeak resolution of 7.6% for photons of energy equal to 662 keV [1].

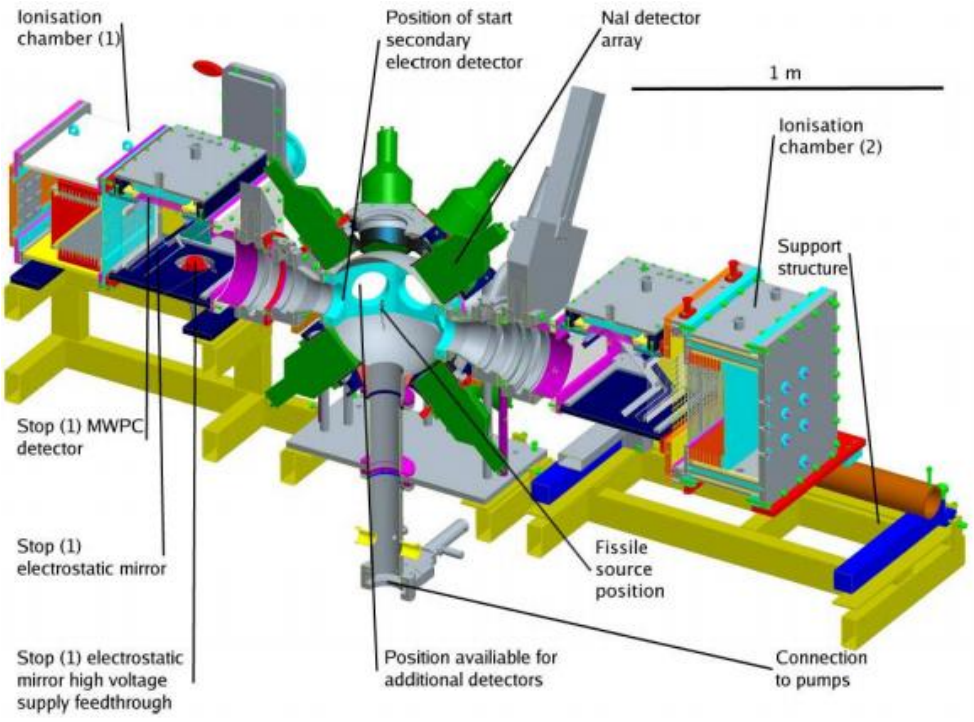

Figure 1.2 – Cross-section of STEFF spectrometer [2].

The spectrometer also consists of sophisticated, nucleus identification apparatus. These combine axial ionisation chambers with digital electronics and secondary electron detectors which can give fragment flight measurements over an approximate distance of 70 cm. These detectors have large fragment acceptance angles giving STEFF a high geometric efficiency of 0.03 sr. The apparatus is designed to give a fission fragment mass resolution, δ_A/A, of 3.5% and an atomic number resolution, $Z/\Delta Z$, of 40 [1].

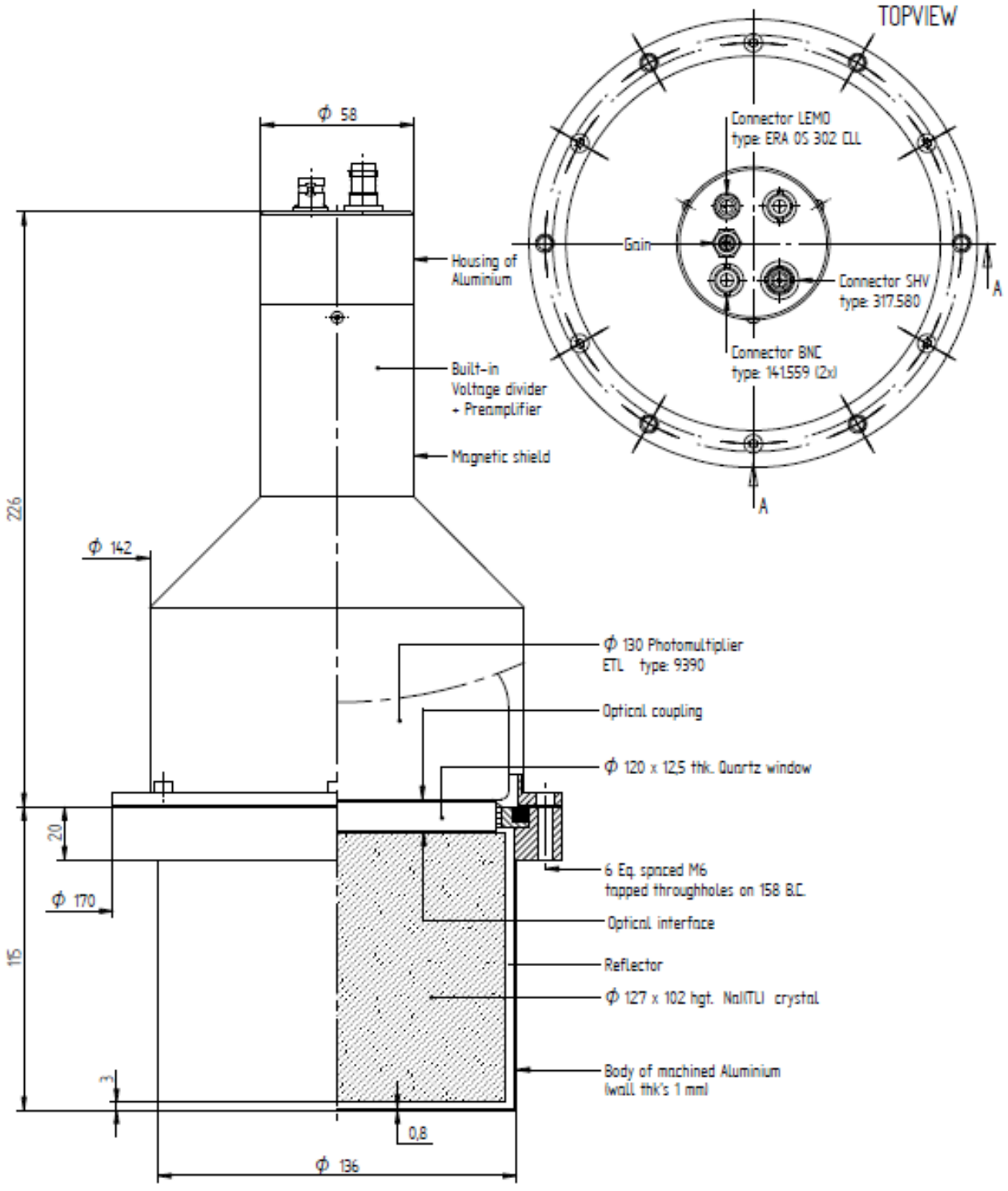

Figure 1.3 – Schematic of NaI detectors used in STEFF [3].

STEFF measures the energies of gamma-rays that are detected by the NaI detectors in coincidence with the fission fragments identified by the nucleus identification apparatus, these measurements are used in conjunction with techniques that assign decay structures to individual nuclei. The goal of these measurements is to study fission fragments created with a low yield that may be produced by reactions taking place within reactors at nuclear energy facilities [1].

2. Computer modelling and the Monte Carlo method

In recent years there has been a significant increase in nuclear science used for both medical and industrial purposes. Medical applications for ionizing radiation have seen a growth both in terms of diagnostic techniques such as radioactive tracers and X-ray imaging devices as well as therapeutic methods such as radiotherapy used for cancer treatments. Industrially, radioactive materials can be used for imaging when it comes to testing the quality of engineering work such as in the building of jet engines or the welding of pipe line, as well as being used to produce energy in the nuclear power industry. The boom in the usage of new technologies in the fields, coupled with their ever more intricate and complex designs, has resulted in the demand for the development of powerful computer simulation software. The new software has to be capable of modelling a wide range of scenarios within large, complicated, three dimensional geometries.

For the following work, Monte Carlo simulations will be made for models involving the transportation of gamma-ray photons [4].

The two most popular techniques used for such software are deterministic and Monte Carlo methods. A comparison of the two methods can be seen in Table 1 taken from [4].

Table 1 - Comparison between Monte Carlo and deterministic methods and codes used to perform the simulation of radiation transport [4].

Item	Deterministic	Monte Carlo
Geometry	Discrete/approximate	"Exact"
Energy Treatment (cross-section)	Discrete (multigroup)	"Exact"
Direction	Discrete/truncated series	"Exact"
Input Preparation	Difficult	"Simple"
Computer Memory	Large	Small
Computer Time	Small	Large
Numerical Issues	Convergence	Statistical
Amount of Information	Large	Limited
Parallel Computing	Complex	Trivial

Deterministic codes use equations to describe the average behaviour of photons within a system. A general equation would give the number of photons as a function of position, velocity and time and would account for any addition of photons from the source and any loss of photons through absorption inside, or escape from the system [5].

The advantages of using the Monte Carlo method is that unlike a deterministic method which makes several approximations in order to try and simplify the problem and calculate the average behaviour of a population, the Monte Carlo method tracks the behaviour and interactions of a single photon within a population as it moves through a system. In doing this, results produced using a Monte Carlo method can be extremely accurate and close to the true nature of a problem provided the input nuclear data is to a high enough degree of accuracy and a large enough number of photons are run [4][5].

There have been significant advances made in the effectiveness and use of computer simulations using Monte Carlo methods. This progress has been aided by the significant development made in the production of computers with

processors of increasing power as well as international efforts made by various laboratories around the world in the collection and storage of data in nuclear cross-section libraries such as the ENDF library [4][6].

The diagram in Figure 2.1, taken from [5], shows the geometry for a simple computer model. Within the model is an area filled with material labelled "Shield", shaded in grey with a thick outline, which can interact with the radiation emitted by the source. A region of interest (ROI) is marked with a thin outline and labelled as "Detector", any photons passing through this area will be tallied in the results of the simulation. The source of the radiation in this model is labelled "Source". These components of the model all exist within the boundaries of a surrounding "World", with limits marked by the dashed line, any space within the world that is not defined as being a material is filled with "void", shaded in white. Any photons moving through this void will have no interaction as there is no material in this region to interact with. Upon reaching the boundaries of the world, a photon will automatically stop being tracked and no results will be produced unless it has passed through the ROI [5].

A Monte Carlo simulation will follow the path taken by an individual photon as it travels through a system using a stochastic method. It uses elements of dice rolling and gaming in order to calculate whether or not the photon travelling through the system will undergo an event. For example, it is not possible to say in which direction a photon will be emitted from a source, only the probability that it will be emitted in that direction, similarly, it is not possible to say where or when a photon will collide with a nucleus within a medium, only the probability whether it will or not. The probabilities used in these calculations are taken from nuclear cross-section libraries, this dependence on experimental data results in a systematic error in the results, the magnitude of which is dependent upon the accuracy of the data taken from the reference library [5].

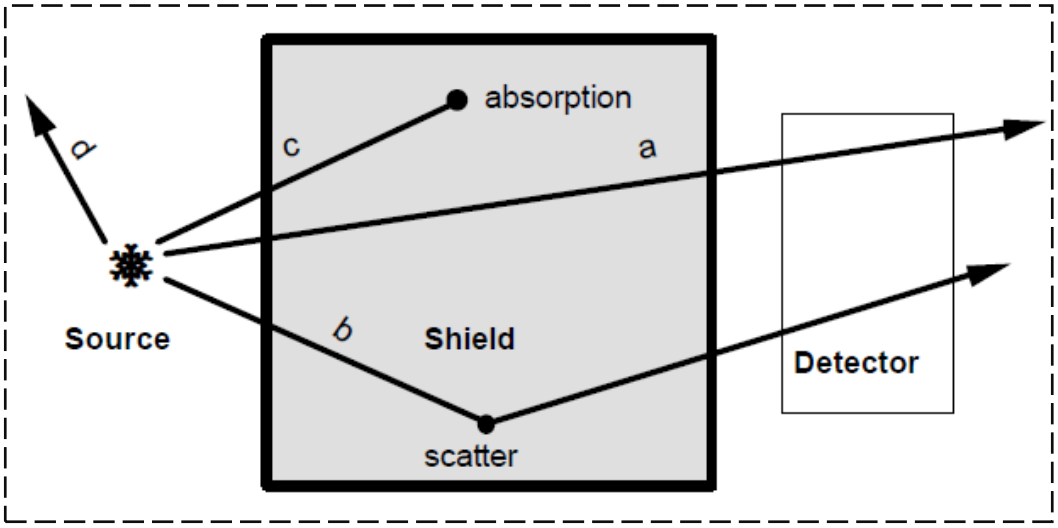

Figure 2.1 – Basic elements of photon transport simulation [5].

Figure 2.1 also shows the four basic paths a photon can take within a radiation transport simulation. Path a) shows how a photon can penetrate through a medium without any interaction. Path b) portrays a photon that enters a medium before being scattered and then continues to travel through the model. Path c) displays a photon entering into the medium and being absorbed. Path d) shows a photon emitted escaping the model without passing through any medium or the ROI. Individual photons can undergo any combination of these events as they travel through the system [5].

A photon's history ceases to be recorded upon being absorbed by material in the model, or passing through the boundaries of the world. After a photon's history stops being tracked, a new photon is emitted from the source and the new photon history is tracked [5].

Some codes have the ability to simulate the production of secondary radiation resulting from the scattering and absorption of the initial radiation produced by the source. Any secondary radiation produced will have its history tracked and any results produced tallied, provided it passes through the ROI [5].

A series of steps is used to track photons within a Monte Carlo simulation [5]:

1. A photon is generated, with its position, velocity and energy dependent on the source description in the input file.
2. The photon's position is tracked as it travels through the geometric model of the system.
3. Positions and outcomes of interactions are calculated depending on the distribution of materials and the data used from the cross-section libraries.
4. Desired results from the photon history, defined in the input file, are tallied.
5. Steps 1 to 4 are repeated for the number of samples that are to be run or the amount of time the simulation is to be run by, as defined in the input file.
6. The tallied results are processed into an output file, with statistical uncertainties calculated for each value.

The Monte Carlo method relies heavily on the use of random numbers when it comes to making a decision on the outcome of a physical event with a range of possible results. The random numbers are generated by the code according to probability distributions, for example, if the radiation emitted from a source is described to be isotropic in a model, then the probability of a photon being emitted in a specific direction is the same as for all other possible directions and so, provided enough samples are run in the simulation, the model would accurately describe the behaviour of a source that emits radiation isotropically in practice [4][5][7].

Probability functions are not always flat. An example of this would be if a source emitted gamma-rays of two different energies and with two different probabilities of emission. This would make the random number generator within the model biased to generating the gamma-ray with the higher emission probability more often. If a large enough number of samples were run, then the observed ratio of different energy gamma-rays emitted by the source would be equal to the ratio of probabilities of emission [4][5][7].

As a result of their dependence on basic statistics and random number generating, Monte Carlo methods obey the law of large numbers. The mean value of a sample is given by Equation 1;

$$\bar{x} = \frac{1}{N}\sum_{i=1}^{N} x_i \tag{1}$$

where the mean value of the sample is $\bar{x}$, N is number of trials used in the sample, and x_i is the result for the ith term. The law of large numbers states that;

$$\lim_{N\to\infty} \bar{x} = \langle x \rangle \tag{2}$$

where ‹x› is the true population mean.

This means the larger the number of trials used in a sample i.e. the larger the number of photons run in a simulation, the closer the simulated result will be to the true value. The trade off for running large numbers of photons however is an increase in computing time [4][5][7].

A simple example of the use of a Monte Carlo method is finding the area of a circle.

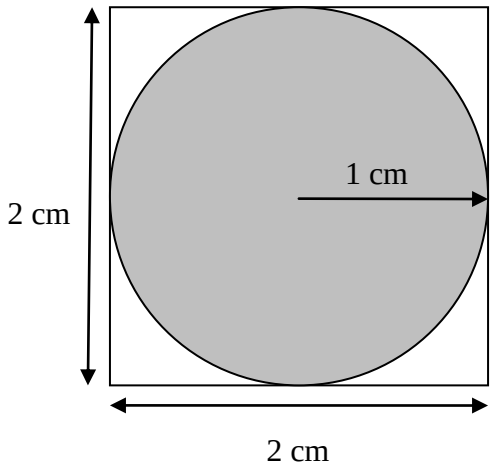

Figure 2.2 – A circle of radius 1 cm inside a square with side length of 2 cm.

Take a circle of radius 1 cm and draw a square around it, with sides of 2 cm length, such that the whole of the circle lies within the square as shown in Figure 2.2. The area of the circle is simply equal to the area of the square multiplied by the ratio of the area of the circle to that of the square, such that:

$$A_C = \frac{A_C}{A_S} A_S \tag{3}$$

where A_C is the area of the circle and A_S is the area of the square. The problem with Equation 3 is that in order to calculate the unknown quantity A_C, is that it requires knowing the value of A_C. Using a Monte Carlo method does not require this previous knowledge. In order to find the area of the circle using a Monte Carlo method, random points, or sample, would be chosen within the area of the square. Any of the samples that also lie within the limits of the circle would be recorded in the results and the area of the circle would be given by the area of the square multiplied the ratio of the number of samples recorded in the results to the total number of samples run, as shown in Equation 4:

$$A_C = \frac{n}{N} A_S \tag{4}$$

where n is the number of samples recorded an N is the total number of samples run. As stated before, the greater the value of N, the closer the calculated value of A_C will be to the true value [5].

2.1 MCBEND

MCBEND is a commercial computer program, developed, supported and distributed within the UK by the ANSWERS software service, formerly part of SERCO but now owned by AMEC. MCBEND uses the Monte Carlo method for particle transport calculations of sub-critical systems. It has the ability to perform neutron, gamma-ray, electron and coupled neutron-gamma calculations, for all of which it simulates the creation, transport and fate of a finite number of particles. MCBEND Version 10A was used for the purpose of this investigation [5][8][9].

The code has been under development by the ANSWERS group for over 30 years. It has been used in applications such as the design of reactor plants, fuel flasks, reprocessing plants, fusion devices and particle accelerators [5].

It utilizes a simple body geometry known as Fractal Geometry (FG) which uses simple, three dimensional geometric shapes such as boxes and cylinders, to make up the building blocks of the geometry of a model. FG uses a combination of these shapes to build bodies arranged into "zones". These zones are combined together to form "parts" with their own local coordinate system. Parts may be included in the construction of subsequent parts any number of times. Arrays of parts can be made, this is useful for problems with systems in which certain geometries are repeated several times, for example, an arrangement of fuel rods could be formed by defining a single fuel rods geometry and then creating an array to repeat the geometry of the fuel rod part as many times as required. Using arrays saves both time and computer memory. All initial parts are then combined into one final part that fully describes the geometry of a system [5][8][10][14].

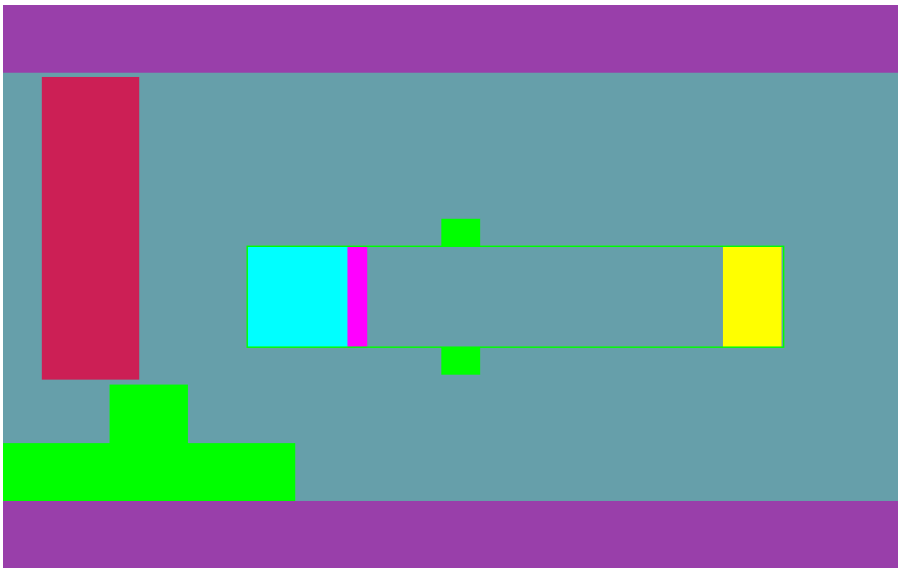

Figure 2.3 – Two dimensional ray display, produced by Visual Workshop, of model defined in Appendix A.

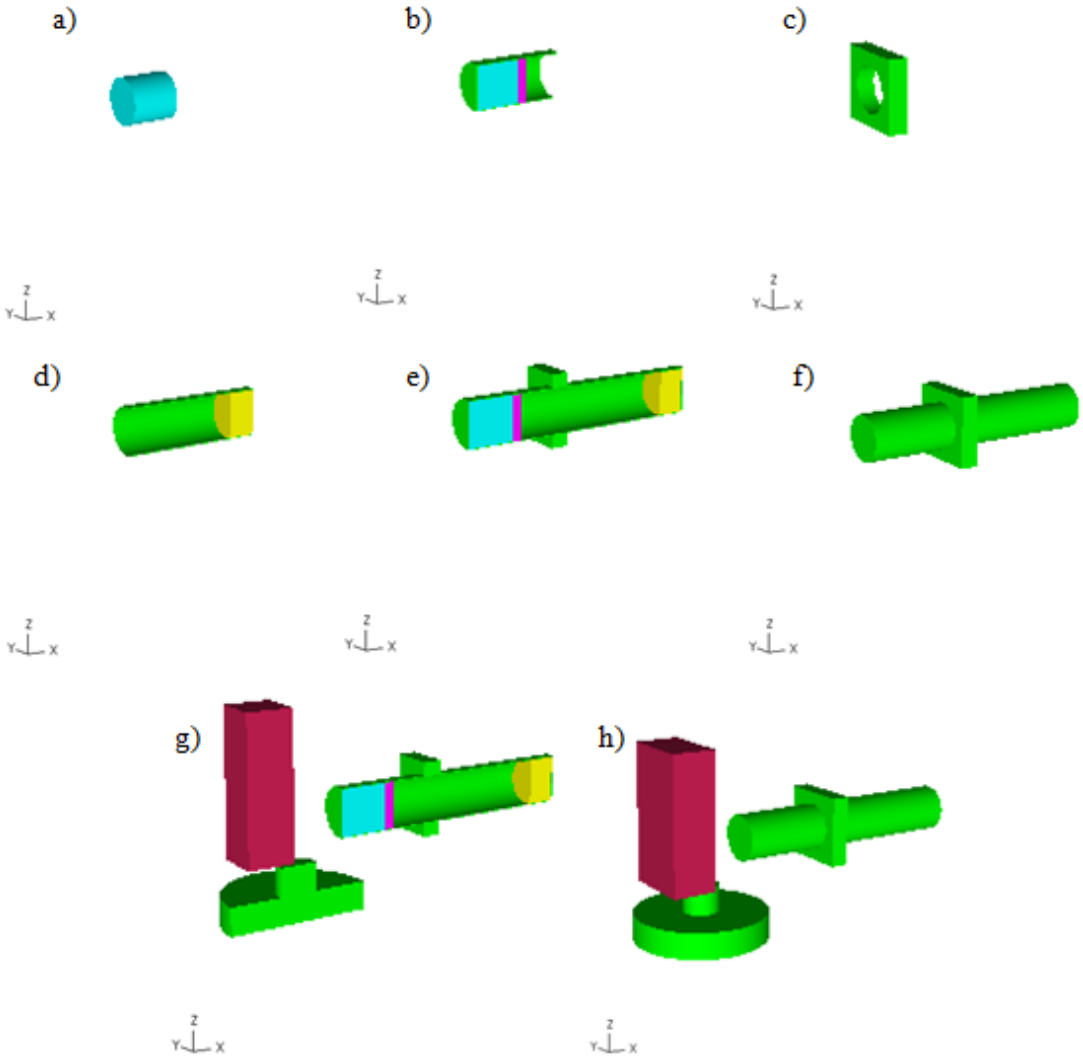

Figure 2.4 – The three dimensional ray output for the model described in Appendix A by Visual Workshop. NaI is shown in turquoise, aluminium in green, glass in pink, iron in yellow and lead in maroon. a) shows part 1 of the model, the crystal on its own. b) shows part 2, the front of the detector, which includes crystal defined in part 1, an aluminium coating and n optical window with some space behind, the image has been sliced so as the interior of the cylinder can be observed. c) shows part 3, the detector mount. d) is part 4 of the model, the photomultiplier tube, this has been modelled as a hollow aluminium cylinder with some iron at the back end to simulate the detectors electronics. e) and f) show a sliced and unsliced view of part 5 respectively, this part combines all previously defined parts of the model into one, the full geometry of the detector. g) and h) show the entire final version of the model, sliced and unsliced respectively. The final version of the model combines the full detector geometry of part 5, an aluminium stand used for the source mount and a lead brick.

Appendix A is an example of a MCBEND input file. Figure 2.3 shows a two dimensional ray image of the model defined in Appendix A. Figure 2.4 shows how several parts are individually constructed before being combined to make the final geometric representation of the model defined in Appendix A, as well as displaying the three dimensional, real-time, interactive visual output provided by Visual Workshop. Figure 2.5 shows the three dimensional wire display produced by Visual Workshop for the model defined in Appendix A.

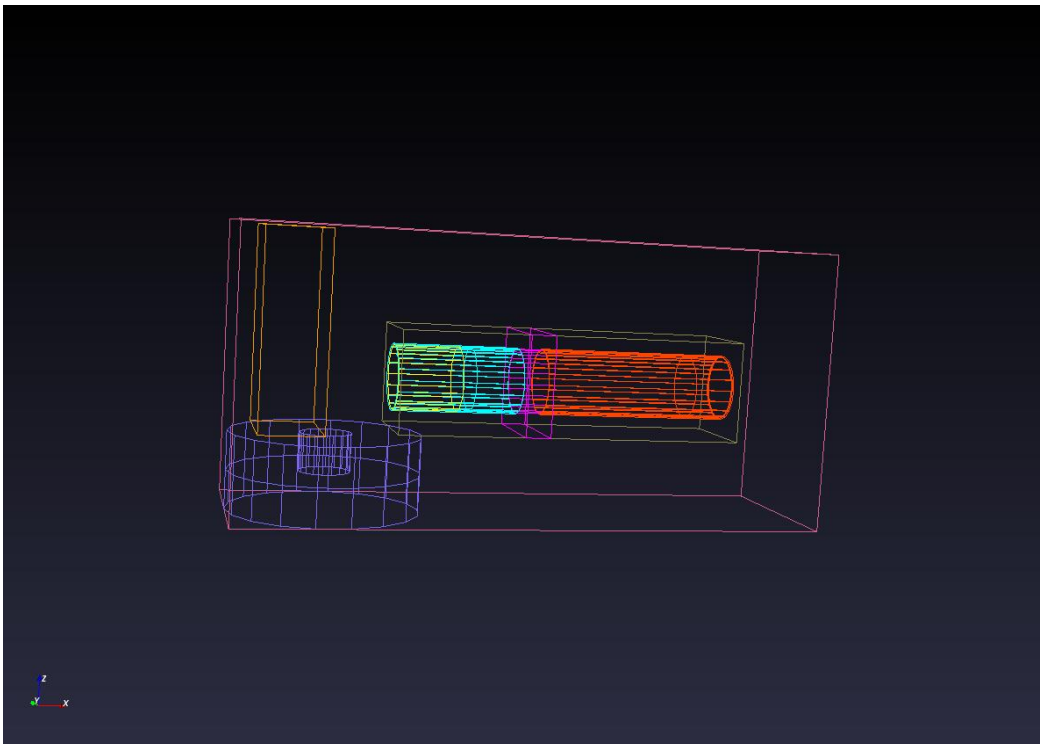

Figure 2.5 – Three dimensional wire display, produced by Visual Workshop, of model defined in Appendix A.

Each basic geometric shape is given a specific material definition by the user. Materials can be defined by custom, user made mixtures of elements or chosen from a list of predefined materials provided by MCBEND [5].

MCBEND uses cross-sections held in 13,193 ultra-fine energy groups for calculations involving neutrons. It uses a module called DICE in order to process neutron collisions and it takes information from various evaluated nuclear data

files such as the JEF2.2 [11], ENDF/B-VI [12] and JENDL3.2 [13] files. An equivalent point-energy library is available for gamma-ray calculations, a module called GAMBLE is used to process the collisions. Charged particle transport uses a condensed history method [5][9][14][15].

The program allows for the modelling of a variety of sources of varying geometries, including point, line, surface and body sources. The sources can also be modelled to have various energy spectra that can be weighted manually, or taken from one of the available in-built spectra [5][9][15].

All results from a MCBEND simulation are presented in an output file with error calculations produced for each result. The program has the ability to run a dump and restart operation which allows for calculations to be run with larger numbers of samples until a satisfactory variance in the results is met [5].

2.2 MCNP

MCNP is a general purpose, continuous energy Monte Carlo N-particle transport code with the ability to perform in several transport modes; neutron only, photon only, electron only, combined neutron/photon where photons are produced by neutron interactions, neutron/photon/electron, photon/electron and electron/photon. Neutron energies can range from 10^{-11} MeV to 20 MeV, photon and electron energies can range from 1 keV to 1000 MeV [6][16].

It was produced by the diagnostics applications group in the applied physics division at the Los Alamos National Laboratory. The version used for the purpose of this investigation was MCNP4C that was released in 2000. The code first emerged under the name MCNP in 1977 but has routes in the first work done on Monte Carlo method computing dating back as far as the 1940's. The accumulative efforts of people working on the code amount to around 500 person-years of work. It now boasts a worldwide community of over 3000 users at more than 260 institutions [16][17].

The applications of MCNP have come far since its beginnings. It was originally designed to solve radiation shielding and criticality safety problems, since then it has been developed to a great enough extent that it can model intricate systems

such as human anatomy and organs, to large scale experiments such as particle accelerator facilities [17].

The MCNP code uses a three dimensional Cartesian coordinates system for the modelling of the geometry of a system. MCNP uses first and second degree surfaces and fourth degree elliptical tori to bind three dimensional volumes or cells, which are then given user defined material definitions. An example of an MCNP input file is given in Appendix B. Figure 2.6 gives an example of the two dimensional visual display generated by MCNP, the geometry shown is the same as the one defined in Appendix B [6][16].

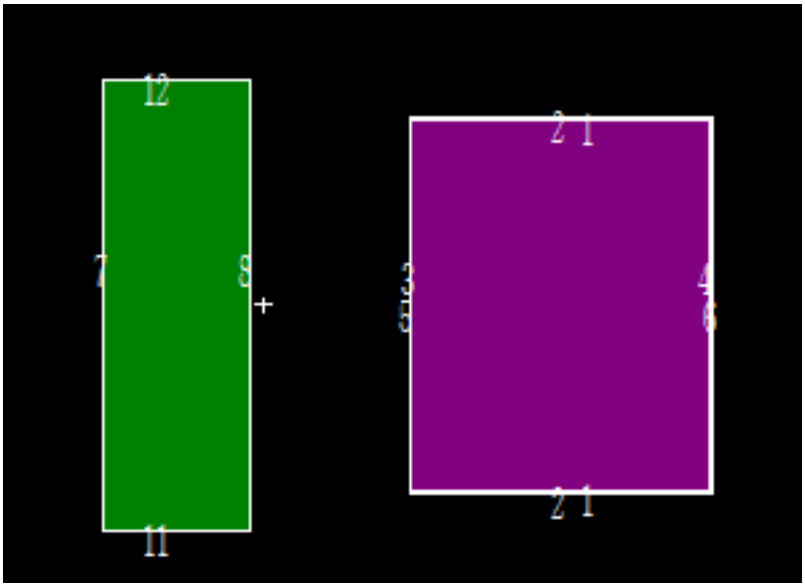

Figure 2.6 – Two dimensional visual output produced by MCNP of the model defined in Appendix B. Lead is shown in green, NaI in purple. The aluminium coating around the NaI crystal is too thin to be seen in this image.

MCNP utilizes continuous-energy nuclear and atomic data libraries with the primary sources for the nuclear evaluated data coming from the ENDF [18], ENDL [19] and ACTL [20] as well as evaluations from the applied nuclear science group at Los Alamos. Evaluated data is processed into formats that can be used by MCNP by codes such as NJOY [21]. There are over 500 neutron interaction tables available for approximately 100 different isotopes and elements,

multiple tables are available for different isotopes due to data being derived from different evaluated files as well as for different temperatures and processing tolerances. Neutron-induced photon production data is included in the neutron interaction tables. [16].

Photon interaction tables exist for elements with Z values ranging from 1 to 94. The data provided in these tables allows for calculations of coherent and incoherent scattering events, photoelectric absorption with the possibility of producing fluorescent emission, pair production with local emission of annihilation radiation and bremsstrahlung [16].

Electron transport calculations use a continuous-slowing-down model that includes positrons, k X-rays and bremsstrahlung. This model does not include external or self-induced fields [16].

MCNP allows for the user to define the source to have point, line, surface or three dimensional body geometries, the location of the source in the world and the energy definition of the source [6][16].

Results for MCNP simulations are given in an output file displaying the desired tallies, with a numerical value and a percentage error on that value. The output file also provides the user with a value for the figure of merit (FoM) of the simulation. The FoM is a measure of the efficiency of the model, calculated by comparing the size of the variances on the results to the computing time of the simulation, as shown in Equation 5 [6][16].

$$FoM = \frac{1}{R^2 T} \tag{5}$$

where R is the relative error and T is the computing time.

2.3 GEANT4

GEANT4 is a software toolkit for the simulation of the passage of particles through matter. It has the capabilities to run simulation for neutrons, photons and electrons, resonant particles with short life times such as vector mesons and delta

baryons, nuclei such as deuteron, alpha and heavy ions and quarks, di-quarks and gluons[22][23][24].

The origins of GEANT4 can be found in two independent studies done at CERN and KEK in 1993. The two projects investigated how modern computing techniques could be used to improve the GEANT3 program used at the time. The result was the birth of the RD44 project, an international effort involving over 100 scientists and engineers from more than 10 facilities worldwide. The first public release of the program was in December 1998, with the GEANT4 Collaboration being established in 1999 to continue with further development and refinement of the code [22][23].

Geometries are formed in GEANT4 by defining volumes. Each volume is formed by describing a shape and the physical characteristics of the shape and then placing it inside a containing volume. This method creates a hierarchy of volumes in which several daughter volumes can exist within a mother volume, provided they do not overlap. Shapes can be defined either by built-in models of solids with simple three dimensional shapes such as boxes, spheres or cylinders in or by combining user defined surfaces in order to create shapes of more complex geometries [24][25].

GEANT4 sources data from several evaluated nuclear cross-section data files. The file used in a calculation depends on the type of particle involved. Libraries utilized include the ENSDF, ENDF/B-VI, SAID, ABLA V3 and EPDL97 files as well as several others [22][24][26].

Source definition in GEANT4 is user defined. The program has the ability to create sources that produce many different types of particles using the G4ParticleGun particle generator, however, more sophisticated source definitions can be made for primary particles using the G4GeneralParticleSource module, which allows the user a much greater control over the source definition. Using this module, multiple independent sources can be used in a single run, the angular distribution of the emission of particles from the source can be dictated and the energy distribution can be defined [24].

3. Experiment

3.1 NaI detectors

There are a number of general properties of radiation detectors that are worth noting before further discussion of the specific detectors used in this project, these are a detectors energy resolution, its detection efficiency and the dead time of a detector. For the discussions in this section, [27], [28] and [29] can be used for a broad, general background reading.

The energy resolution of a detector is an important feature of any detector, it determines the shape of the peaks in a measured spectrum. The energy resolution is given by Equation (6):

$$R = \frac{FWHM}{E_0} \tag{6}$$

where R is the energy resolution, $FWHM$ is the full-width half maximum of a specific peak, and E_0 is the energy of the peak. A "good resolution" will result in peaks of greater height and smaller FWHM, this is beneficial when identification of peak energies is of importance. Semiconductor detectors typically have energy resolutions of less than 1% and scintillator detectors, such as the ones used in this project, have resolutions of 5-10% [30].

The detection efficiency of a detector is equal to the ratio of photons detected by to the total number of photons incident on the detector. The efficiency of a detector is dependent on many factors, the material of the detector has an effect depending on how easily the radiation interacts with it, the energy of the incident radiation also is important, particles with higher energies have longer mean free paths and so travel further before taking part in an interaction. This also implies that the thickness of the detector in the direction of the radiation is a factor that needs to be taken into account, larger detector dimensions will result in higher detector efficiency [30].

The dead time of a system is the minimum period of time that must separate two events in order for them both to be recorded as two separate pulses. The dead time can be caused by either physical processes within the detector itself, or processes in the electronics of a system. The period of time measurements are taken over is called the real time, the amount of time in which actual results are recorded is called the live time, the dead time is the amount of time when results cannot be recorded due to other results being processed in the system, it is usually given as a percentage. The dead time of a system can become a problem when high count rates are encountered [27].

The STEFF project and the following experiments made extensive use of NaI detectors. NaI detectors are scintillation devices that are used for the detection of gamma-rays [30].

Scintillation detectors are made by coupling a piece of scintillating material with a photomultiplier tube (PMT) as shown in Figure 3.2. Ideal scintillating material possesses the following properties [30]:

- The ability to convert a photon's kinetic energy into detectable light with high scintillation efficiency.
- The conversion of kinetic energy into detectable light should be linear – light yield should be proportional to the deposited energy over a wide range.
- The material should be transparent to the wavelength of light of its own emission, allowing the light produced to reach the detector at the back of the material.
- The induced luminescence should have a short decay time, allowing for the generation of fast signal pulses.
- The material should have good optical quality and be able to be manufactured into sizes large enough to be used as practical detectors.
- The refractive index of the material should be close to that of glass (≈1.5) so as to allow for efficient coupling of the scintillation light to the PMT.

No material simultaneously meets all these criteria and making the choice of which scintillating material to use comes at a compromise among these factors, dependent on what applications the detector will be used for [27].

NaI is an inorganic scintillating material; inorganic scintillators have a greater light output and linearity than other types of scintillator at the cost of producing slower response times. The high Z-values and densities of inorganic scintillators make them the most popular choice for gamma-ray spectroscopy. NaI is the most popular inorganic detector because of its large photon absorption probability due to the large Z value of the iodine (Z=53), as well as it being relatively cheap and easy to produce in large crystals [30].

Electrons in inorganic scintillating crystals exist in discrete energy bands. The two highest energy bands are the valence and conduction bands as shown in Figure 3.1. Valence band states are generally full and conduction bands empty, allowing for electrons in the valence band to be excited into the empty states in the conduction band by interacting with radiation of sufficient energy to bridge the energy gap between the two bands. Excited electrons then fall back into the valence band by losing energy through the emission of a photon, these photons tend to have energies greater than that of the visible light that the photocathode in the PMT is sensitive to [30].

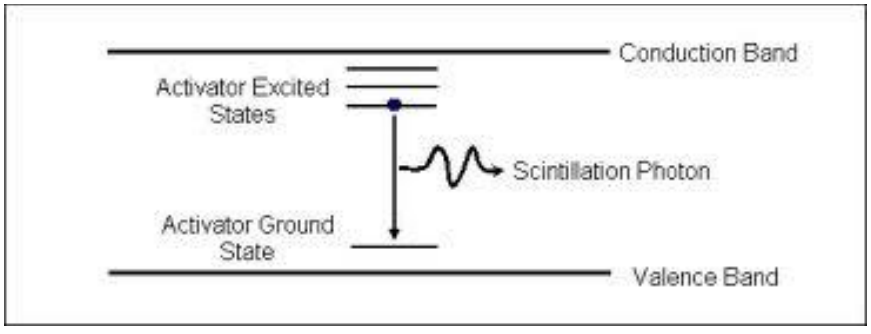

Figure 3.1 – Energetic states of electrons in a scintillator detector with an activator.

In order to shift the photon wavelengths back towards those of visible light, impurities such as thallium are often added to the scintillator crystal. The impurities, called activators, provide vacant energetic states between those of the conductance and valence bands for the electrons to occupy as shown in Figure 3.1. These energetic states become occupied by electrons in the conductance band as they lose energy through photon emission. Photons emitted by such electrons have longer wavelengths than the photons that would fall back into the valence band of the scintillating material, for example, in a NaI(Tl) detector, the photons emitted by the de-excitation of electrons would have a wavelength of 410 nm which is in the region of visible light, whereas a pure NaI detector would produce photons with wavelengths of 303 nm which is ultraviolet. This shift in wavelength also means that the photons cannot be reabsorbed by the NaI crystal as the photons do not have sufficient energy to excite electrons from the valence to the conductance band and they cannot be reabsorbed by the thallium as its ground states remain vacant [30].

As well as showing the schematic of a typical scintillator detector, Figure 3.2 shows the paths taken by photons upon entering the detector. Incident gamma-ray photons enter the detector and transfer all or part of their energy to electrons or electron-positron pairs through either the photoelectric effect, Compton scattering or pair production. This deposition of energy within the scintillating material causes electrons to enter excited states, electrons in these states then de-excite by emitting a visible or near-visible light fluorescent photon which is then directed towards the photocathode which in turn produces photoelectrons that then enter the PMT [30].

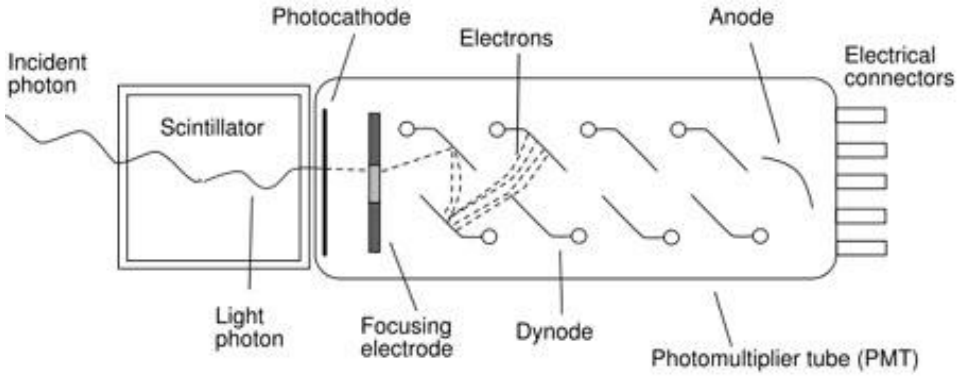

Figure 3.2 – Schematic of typical scintillator detector and the path of incident radiation as well as prompt photons and electrons.

The PMT works by applying a large voltage gradient between the photocathode, a series of electrodes called dynodes and an anode at the back end of the PMT. The electric field produced causes the photoelectrons produced by the photocathode to be accelerated towards the first dynode, they are focused onto the surface of the dynode by a focussing electrode. The electrons incident on the surface of the dynode have sufficient energy to release multiple secondary electrons, the number of which depends on the potential difference applied across the PMT. These electrons are then accelerated towards the second dynode where they then release further electrons which are then accelerated to the next dynode and so on until the final cascade of electrons are incident upon the anode. As many as 5 electrons can be released at each dynode giving a ten-stage PMT an overall amplification factor of 5^{10}. The result of this electron multiplication is the production of a small pulse of current which can be further amplified and processed by further electronic systems.

The various types of interaction that the gamma-ray photons have with the matter have an effect on the structure of the spectrum produced, Figure 3.3 shows the response of a detector to a gamma ray of energy E_γ.

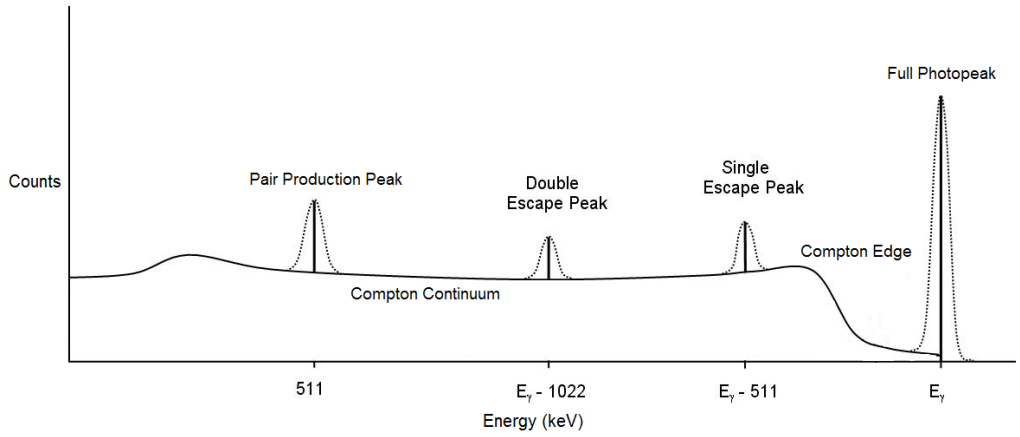

Figure 3.3 – Response of a detector to gamma rays of energy Eγ.

The photoelectric effect is responsible for the production of the full photopeak, it is formed after the photon's energy is fully deposited in the detector. This occurs when the photon undergoes photoelectric absorption by an electron in one of the inner atomic shells of the detectors material, the electron is then released with kinetic energy given by Equation 7 [31]:

$$T = E_\gamma - B_e \tag{7}$$

where T is the kinetic energy, E_γ is the photon's energy and B_e is the electron's binding energy. The atom from which the electron is released is left in an excited state. It can de-excite by electrons in higher energy shells falling down into the vacant states and so releasing a characteristic fluorescent X-ray which may also be detected and produce a peak in the spectrum, or by releasing subsequent, less tightly bound electrons. Electrons released in this process are known as Auger electrons [31].

The Compton edge and Compton continuum features are a result of the radiation photons undergoing Compton scattering. Compton scattering involves a photon being scattered by an electron in the detector material. The photon loses some of its energy to the electron which then recoils with kinetic energy given by Equation 8 [32]:

$$T = E_\gamma - E'_\gamma = E - mc^2$$

(8)

where T is the kinetic energy of the recoiling electron, E_γ is the incident photon's initial energy, E'_γ is the photon's energy after scattering, E is the total energy of the recoil electron including its rest mass energy mc^2. Conservation of momentum rules require the photon's initial momentum p_γ, to be added vectorially to form a closed triangle with the scattered photon's momentum p'_γ and the recoil electron's momentum p. Using the cosine rule Equation 8 can be written [32]:

$$(pc)^2 = E_\gamma^2 + (E'_\gamma)^2 - 2E_\gamma E'_\gamma \cos\theta = E^2 - (mc^2)^2$$

(9)

where θ is the angle of scattering as shown in Figure 3.4.

Figure 3.4 - Diagram of a photon coming in from the left and being scattered off an electron by an angle of θ.

By combining Equation 7 and 8 it is possible to eliminate E and write an expression for the scattered photon's energy [32]:

$$E'_\gamma = \frac{E_\gamma}{1 + \left(\frac{E'_\gamma}{mc^2}\right)(1 - \cos\theta)}$$

(10)

As the photons can be scattered by a continuum of angles ranging from 0˚ to 180˚, the resulting energies are also continuous in nature ranging from a maximum value of E'_γ when θ = 0˚ to a minimum value at θ = 180˚. The Compton edge is produced when the transfer of energy by the incident photon is at a maximum but is not absorbed by the detector. This happens when the photon is scattered by 180˚, the energy of such events are given by [32]:

$$E_{Compton} = \frac{2E_\gamma^2}{mc^2 + 2E_\gamma} \tag{11}$$

The final features in Figure 3.3, the single escape, double escape and the pair production peaks are produced by the pair production interaction. This may only occur when a photon has energy greater than the rest mass energy of an electron and positron, 1022 keV. At energies greater than this it is possible for a photon to convert into an electron and positron pair with total kinetic energy given by [33]:

$$T_- + T_+ = E_\gamma - 2mc^2 \tag{12}$$

where T_- and T_+ are the kinetic energies of the electron and positron respectively, E_γ is the energy of the incident photon and mc^2 is the rest mass energy of an electron/positron [33].

The single and double escape peaks are produced as a result of electron-positron pair production taking place in the material of the detector crystal. After the pair is produced, the electron enters a vacant state and so deposits its kinetic energy, the positron will annihilate with an electron in the detector material and so release two photons both with energies of 511 keV. The single escape peak is produced when one of these two photons escapes the detector and so a total 511 keV of the initial photon's energy is not deposited and so not measured. This results in the single escape peak being produced at a E_γ-511 keV along the energy spectrum. The double escape peak is a result of both the annihilation photons escaping the detector and so the peak will be formed at E_γ-1022 keV.

The pair production peak is produced by pair production and subsequent positron annihilation occurring in material surroundings of the detector, with one of the annihilation photons produced depositing all of its energy in the detector.

More precise gamma-ray detection devices are available in the form of semi-conductor germanium detectors, however, as the purpose of the following work is in aid of the STEFF project which utilizes NaI detectors, the following work was also done using NaI detectors [30].

3.2 Modelling of ^{60}Co decay with MCBEND

The structure of a ^{60}Co gamma-ray decay spectrum was measured experimentally using a NaI detector. This was done to see if the complete structure of the observed spectrum could be modelled accurately, the main feature of interest being the sum peak caused by the simultaneous detection of the two gamma-rays produced in the decay, by the detector.

Experimental spectra were taken for the decay of a ^{60}Co source using a NaI detector attached to a high voltage supply of 780 V. The detector's NaI crystal was cylindrical and had a depth and diameter equal to 51 mm. A detector of this size was used instead of a STEFF NaI detector due to the ones used in STEFF not being available in the lab in Manchester, they were being used on experiment in Grenoble at the time. Signals from the detector were then sent through an amplifier with gain settings such that the full structure of the sum peak could be observed, then finally processed by the multichannel analyser software package, MAESTRO.

A decay scheme for ^{60}Co is given in Figure 3.4. ^{60}Co has a 5^+ ground state that decays primarily by beta decay into a 4^+ excited state of ^{60}Ni which then de-excites to a 2^+ state by emission of a 1.173 MeV gamma-ray and then to a 0^+ ground state by emission of a second gamma-ray of energy 1.332 MeV. The 2^+ state of the ^{60}Ni is short lived and so the 1.332 MeV gamma-ray is emitted almost instantaneously after the 1.173 MeV gamma-ray. Due to this almost simultaneous emission, there is a chance that both gamma-rays will enter the detector at the same time and deposit their full energies, resulting in the production of a sum

peak. The probability of this happening is dependent on the solid angle of the detector which is inversely proportional to the square of the distance between the source and the detector.

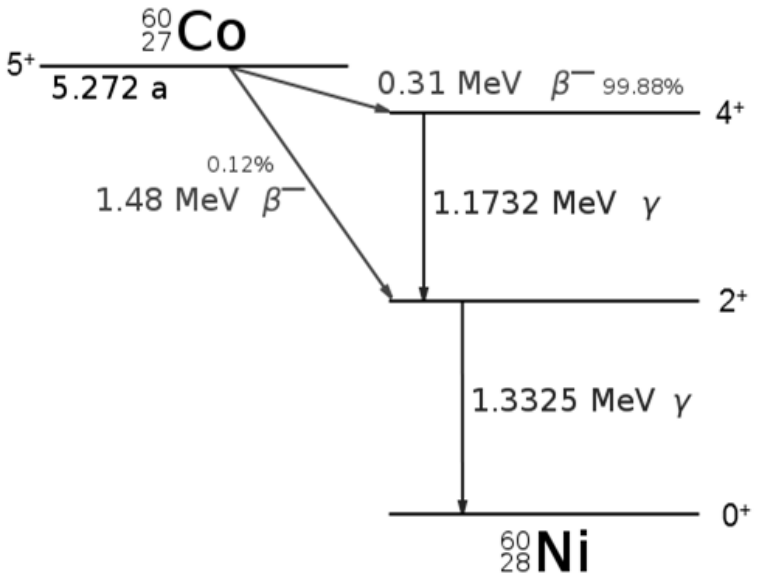

Figure 3.5 – Decay scheme for ^{60}Co.

Firstly, a spectrum of the background radiation of the lab was taken. This would then be subtracted from the spectrum taken of the ^{60}Co decay, so that the final spectrum's structure would be created purely by the radiation emitted by the source. Results were taken for a period of 3001 seconds live time.

The detector was placed a distance of 3 cm from the source so as to produce spectra with clear sum peaks with good statistics. The source was not placed right next to the detector to avoid overloading the electronics of the system that would result in long periods of dead time.

A spectrum of the ^{60}Co decay was then taken. Results were taken for a period of 2367 seconds live time.

The results for the ^{60}Co and background spectrum were then normalised with respect to time and the normalised background spectrum subtracted from that of the normalised ^{60}Co.

A simplified model of the experiments geometry was made using MCBEND. This geometry included the NaI detector used in the experiment and an aluminium mount that the source was held in. The source was modelled as a point source, emitting radiation isotropically.

MCBEND runs were made using batch sizes of 10 million samples. Two separate spectra were produced for single line gamma-ray energies of 1.173 MeV and 1.332 MeV. These single line spectra were then put through a broadening process by the program Resbroad, the source code of which can be seen in Appendix C. Resbroad works by taking the Full-Width Half Maximum (FWHM) of peaks in a spectrum as a quadratic function of energy, the quadratic function is then input into the control file as well as the names of the input file and output file. The input files format must have two columns, one for energy the other for the counts per energy bin. Resbroad then takes the information provided by the user and produces a Gaussian broadening on the line spectra.

In order to produce the effects of the sum peak observed in the experimental results, a small code had to be written in c++ called CoSpec. The source code for CoSpec can be seen in Appendix D.

CoSpec works by taking two monoenergetic spectra of different energies, produced from running simulations by codes such as those mentioned in Section 2 and combining them to create a sum event spectrum. The two spectra used in the calculation of the sum event spectrum must have energy bins of equal size. The input file formats for CoSpec should be in one column and contain the values of the probability of a count being recorded in a specific energy bin, arranged in order of ascending energy. This probability, which will be referred to as the alpha value, is calculated by taking the total number of counts made in a specific energy bin and dividing through by the total number of samples used, i.e. if a run uses 10

million samples and 10 thousand counts are made in a specific energy bin, the α value for that bin will be equal to 0.001.

CoSpec then produces an output file with one column of results for the alpha value for each energy in ascending order for a sum event spectrum. The energy bins for the output file are the same size as the ones used for the input files.

Let the two spectra used to calculate the sum event spectrum be called *1* and *2* and the sum event spectrum called *3*. Let *i* denote a certain energy in *1*. The alpha value for *3* in energy bin *n* can then be calculated as shown in Equation 13:

$$\alpha_{3_n} = \sum_{i=1}^{i=n-1} (\alpha_{1_i} \alpha_{2_{n-i}}) \tag{13}$$

where α_{1_i} is the alpha value for energy bin *i* in *1* and $\alpha_{2_{n-i}}$ is the alpha value for energy bin *n-i* in *2*.

3.3 Comparison of MCBEND, MCNP and GEANT4 simulations

The three Monte Carlo codes MCBEND version 10, MCNP4C and GEANT4 were compared. This was done in order to find which would be the best to use in the creation of a gamma-ray energy reference library.

In order to do this, all three codes were used to make models of identical geometries. The geometry used was that of a STEFF NaI detector, with a point source placed 5 cm away from the front face of the detector.

Runs were made with a lead brick placed 0.5 cm behind the source in order to compare how the models differed in their abilities to deal with back-scatter and the possible production of fluorescent X-rays by materials.

The runs were made for a ^{60}Co decay with gamma-rays of energy 1.173 and 1.332 MeV. The results were put under identical broadening operations and sum events calculated by CoSpec.

The simulations for all three codes were run with a batch size of 10 million samples. Results were tallied in energy bins of width 1 keV.

3.4 Production of the gamma-ray energy reference library and the structure of a ^{152}Eu spectrum

The aim of this part of the experiment was to produce a reference library of spectra that could be used in the future by the STEFF research group. The library will be of use for processes such as future analysis of complex decay spectra which may include unknown gamma-ray transition energies, spectra in the library can be scaled appropriately instead of computer simulations being run for specific peak energies indentified on an experimental spectrum. A ^{152}Eu decay spectrum was modelled using MCBEND and compared to experimental results to explain how the reference library may be used in future by the STEFF research group.

The MCBEND code was used to produce a gamma-ray energy spectrum library for photons of energies increasing from 50 keV to 1500 keV in intervals of equal energy spacing. The models used to create the library used a STEFF detector geometry, with a point source placed 23.5 cm away from the detector as would be the case during experiment.

The purpose of the library will be to analyse unknown experimentally measured spectra by stripping it down and observing any parts of the spectrum's structure that cannot normally be observed in the full spectrum.

This would be done by first identifying energies of photopeaks along the measured spectrum. Next, the spectrum with the closest energy to the observed identified energy would be chosen from the reference library. This spectrum would then have its energy fit scaled up the appropriate amount. The scaling factor would be given by:

$$S = \frac{E + \Delta E}{E} \tag{14}$$

where S is the scaling factor, E is the energy of the reference spectrum's photopeak and ΔE is equal to the experimental spectrum's photopeak energy, minus the reference spectrum's energy. All the energies along the reference spectrum would be multiplied by the scaling factor, S.

The new, scaled reference spectrum would then undergo an appropriate broadening and then have counts within each channel scaled so as the heights of the experimental and reference spectra's photopeaks would be equal. The reference spectrum would then be subtracted from the experimental spectrum and the process repeated for as many identifiable energy peaks in the experimental spectrum's structure.

The size of the energy intervals between each spectrum in the reference library was decided by making runs for gamma rays of various energies. Results were then overlapped by scaling runs of different photon energies to see how well they overlapped. The size of the energy gaps between each reference spectrum in the library were then chosen by finding energy gaps with as large a gap between spectrum photopeak energies as possible, whilst still providing a decent spectrum overlap in order to produce a library with a small storage demand.

All runs for the library used batch sizes of 10 million samples and results were tallied in energy bins of width 1 keV.

MCBEND was then used to construct a ^{152}Eu spectrum, line energy spectrum. This was done by using published energies and intensities taken from [34], to run simulations for single line spectra with photopeak energies equal to the most prominent known gamma-ray energies observed in the decay of ^{152}Eu. The height of the photopeaks were then adjusted according to the known intensities of the observed gamma-rays. This was done in order to highlight how gamma-ray peaks of low intensity may not be observable in complex spectra if the detectors used have a poor energy resolution.

4. Results and Discussion

4.1 Modelling of ^{60}Co decay with MCBEND

The spectrum for the ^{60}Co decay was taken and analysed using the MAESTRO multichannel analyser program. An energy calibration was made by identifying peaks along the spectrum as regions of interest and assigning a value of energy to them. MAESTRO then provided a linear relationship between the energy and the channel number results were recorded in, of the form:

$$y = ax + b \tag{15}$$

where y is the energy, x is the channel number and a and b are constants arising from the linear fit produced by the MAESTRO program.

The spectra for the background radiation in the lab and the ^{60}Co source were both taken on the 29/03/2012. As the settings on the electronics were not changed between taking results for both spectra, the same energy fit was used for the background radiation spectrum as the one produced by the ^{60}Co spectrum energy calibration.

The background radiation spectrum taken can be seen with counts as a function of energy in MeV in Figure 4.1 on a linear scale and Figure 4.2 on a logarithmic scale.

The spectrum taken of the ^{60}Co decay placed 3 cm from the surface of the detector can be seen in Figure 4.3 on a linear scale and Figure 4.4 on a logarithmic scale.

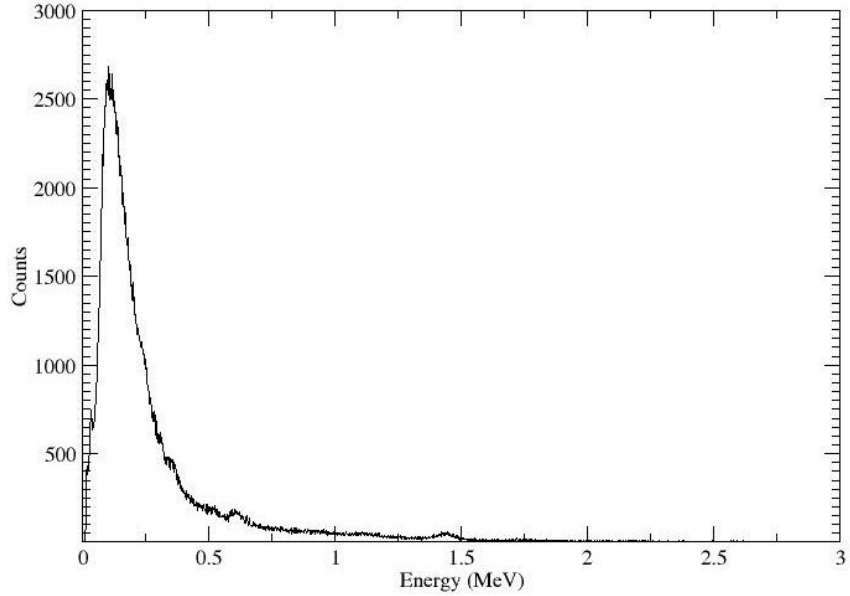

4.1 – Background radiation of lab taken on 29/03/2012. Counts are shown on a linear scale along the y axis as a function of energy along the x axis in MeV.

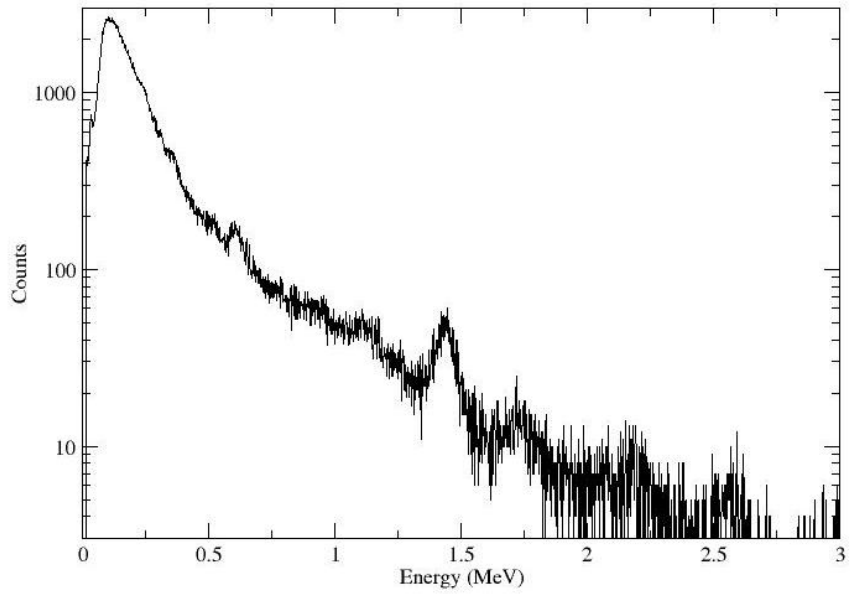

Figure 4.2 - Background radiation of lab taken on 29/03/2012. Counts are shown on a logarithmic scale along the y axis as a function of energy along the x axis in MeV.

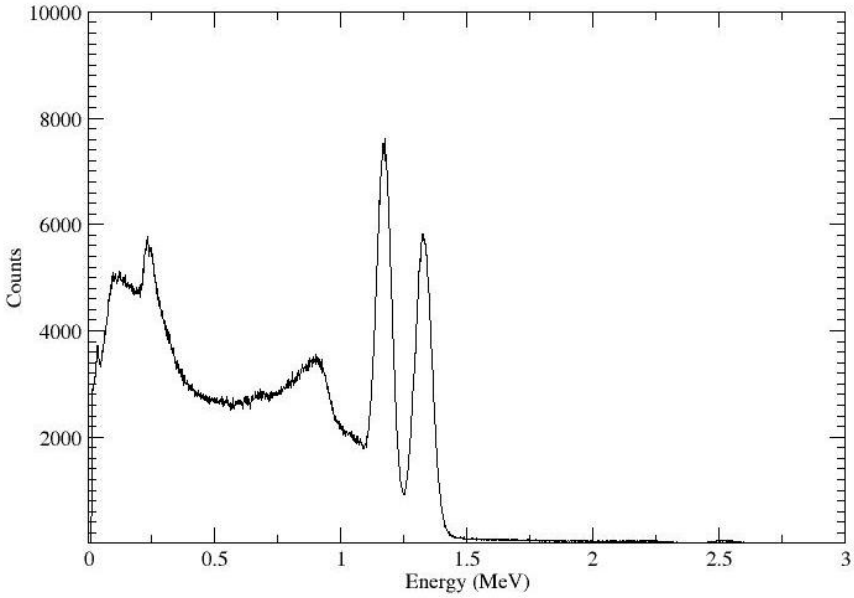

Figure 4.3- Spectrum for ^{60}Co decay taken on 29/03/2012. Counts are shown on a linear scale along the y axis as a function of energy in MeV along the x axis.

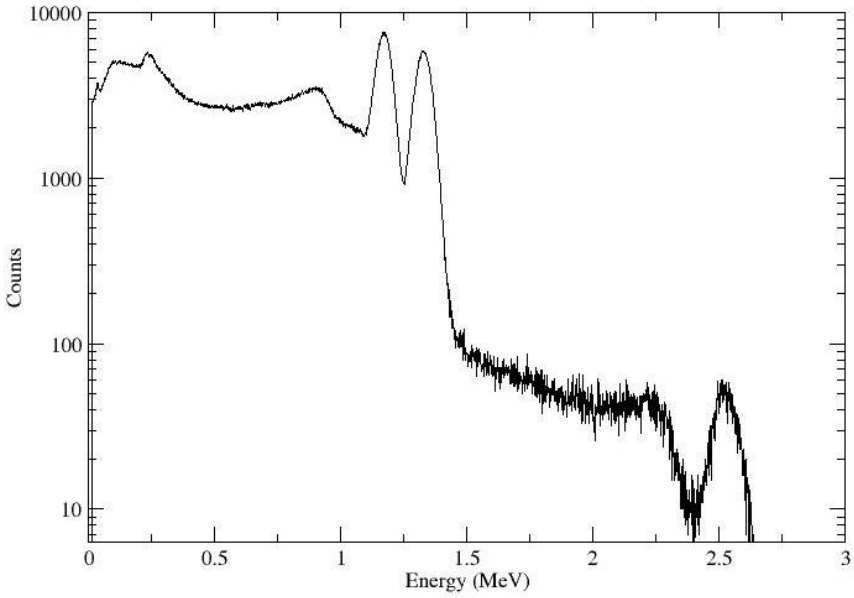

Figure 4.4 – Spectrum for ^{60}Co decay taken on 29/03/2012. Counts are shown on a logarithmic scale along the y axis as a function of energy in MeV along the x axis.

Figures 4.5 and 4.6 show the spectrum for the ^{60}Co with a background radiation subtraction, on a linear and logarithmic scales respectively. After the background subtraction, the spectrum has been normalised to the 1.173 MeV peak value.

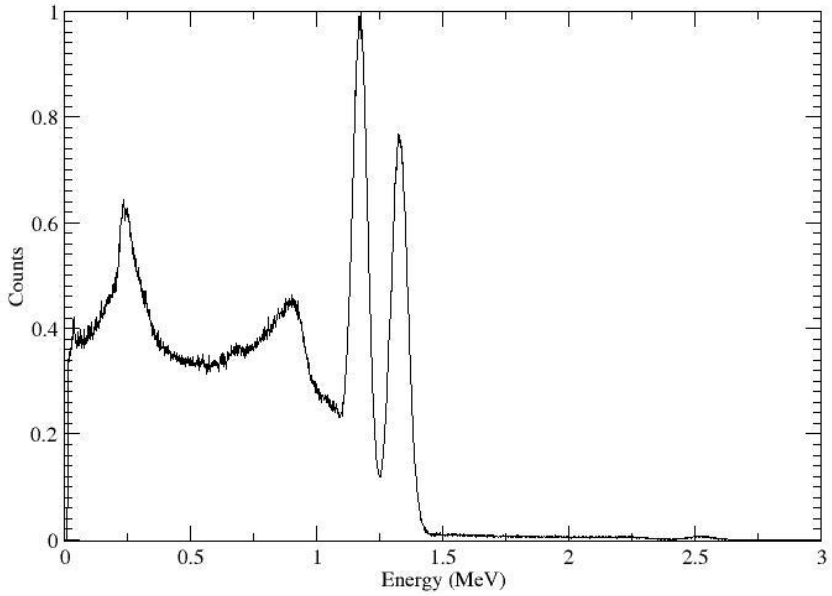

Figure 4.5 – Spectrum for ^{60}Co decay with background radiation subtraction. The results have been normalised to the 1.173 MeV peak value . Counts are shown on a logarithmic scale along the y axis as a function of energy in MeV along the x axis.

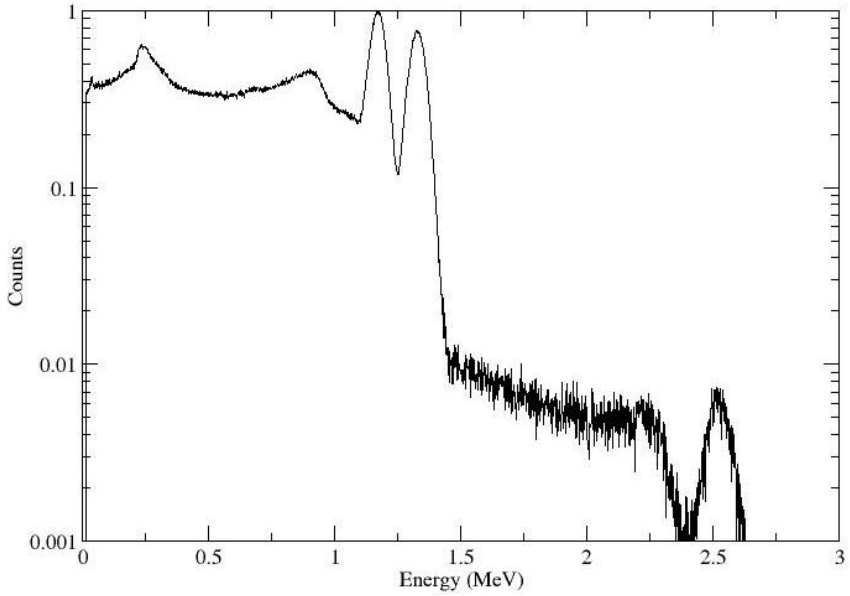

Figure 4.6 – Spectrum for 60Co decay with background radiation subtraction. The results have been normalised to the 1.173 MeV peak value. Counts are shown on a logarithmic scale along the y axis as a function of energy in MeV along the x axis.

Figures 4.7 and 4.8 show linear and logarithmic scale graphs respectively of the spectra for the experimental results and the results of the MCBEND simulation after undergoing the broadening function by Resbroad and the CoSpec sum event spectrum production.

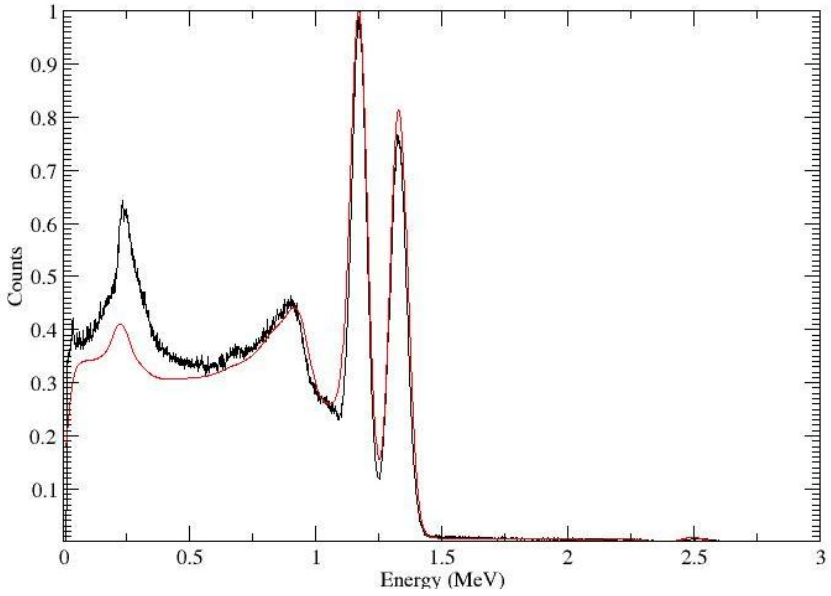

Figure 4.7 – Experimental results shown in black and MCBEND simulation results shown in red for ^{60}Co source. The results have been normalised to the 1.173 MeV peak value. Counts are shown on a linear scale along the y axis as a function of energy in MeV along the x axis.

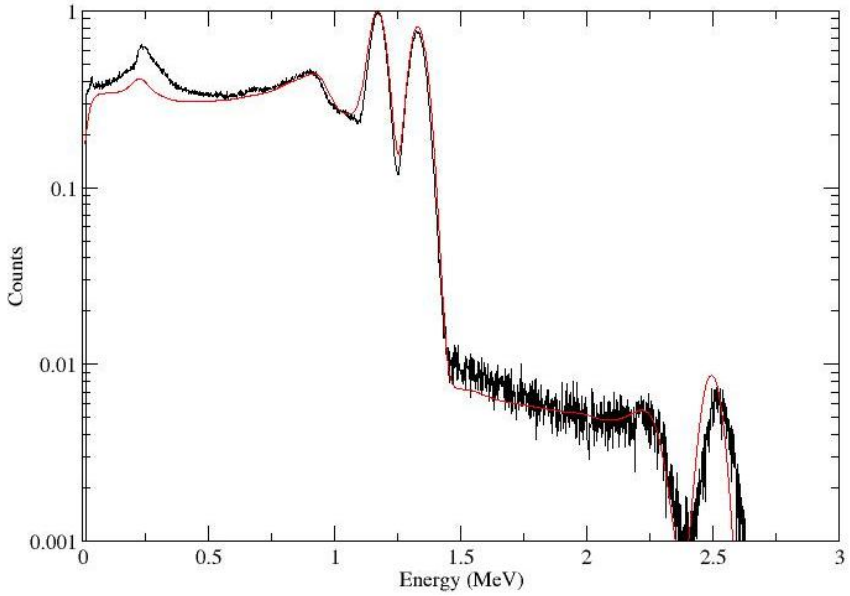

Figure 4.8 – Experimental results shown in black and MCBEND simulation results shown in red for ^{60}Co source. The results have been normalised to the 1.173 MeV peak value. Counts are shown on a logarithmic scale along the y axis as a function of energy in MeV along the x axis. The sum peak energies do not perfectly overlap due to a calibration error for the experimental results.

The results for the experimentally retrieved and MCBEND produced spectra can be seen to overlap well for the 1.173 MeV and 1.332 MeV photopeaks as well as the 2.505 MeV sum peak. The height of the sum peak for the modelled results is slightly greater than that of the experimental results, this could be due to low statistics in the experimental results.

The centroids of the sum peaks of the two spectra do not perfectly align due to the energy fit for the experimental results not being perfect. This could be improved by getting a better energy calibration for the apparatus by using a source with more than two identifiable peaks, so as to give more reference points to calculate with. An attempt was made at making an energy calibration that included the 2.505 MeV sum peak, however the statistics are very low and the energy fit produced was worse.

The Compton continuum of the two spectra overlap well at the high energies nearing the Compton edge however at the lower energies near the backscatter peak, the experimental results have a greater number of counts than the modelled ones by a factor of approximately 1.6. The extra backscatter seen in the experimental results will be from the detectors surroundings in the lab. In the MCBEND model much of these surroundings were not included in order to make the geometry of the model simpler and so reduce the computing time of simulations.

This lack of counts in the Compton continuum is also the reason why the models results are lower for the continuum observed between the 1.332 MeV photopeak and the 2.505 MeV sum peak.

The centroids of the backscatter peaks for the two spectra do not align. As with the sum peak, this is due to a non-perfect energy fit. The centroids of the two full photopeaks for the 1.173 and 1.332 MeV gamma-rays align well as these were the peaks used in the energy calibration of the experimental results.

The results for this experiment would be improved by making an energy calibration for the experimental spectra using more than two reference points for

the fit, this would allow for better alignment of experimental and modelled results centroids.

Adding more material surrounding the detector, for instance the table the detector was stood on, to the MCBEND model would add more counts in the backscatter region of the Compton continuum and so produce a better overlap between the two spectra. It appears that the calculations used by CoSpec for the production of a sum event spectrum work well, as the sum peak and the other sum events, the counts seen in energy bins greater than those of the 1.332 MeV photopeak, overlap well and that discrepancies between the two results could be eliminated by adding more material to the model and taking experimental results for longer periods of time in order to give better statistics for the sum peak.

4.2 Comparisons of MCBEND, MCNP and GEANT4 simulations

Figures 4.9 and 4.10 show comparisons between the three different Monte Carlo codes using a STEFF detector crystal geometry and a lead brick placed 0.5 cm behind the source with counts plotted as a function of energy in MeV on a linear and logarithmic scale respectively. The results for MCBEND are shown in black, MCNP in red and GEANT4 in green. The results all come from simulations using batch sizes of 10 million samples and so the data is already normalised. The results for the GEANT4 simulations were provided by a second party.

There are noticeable differences between the three models. The most obvious of which is the difference in full photopeak height visible in Figure 4.9. MCBEND and MCNP overlap well with almost identical number of counts for both the 1.173 MeV and 1.332 MeV photopeaks however the GEANT4 results give a much shorter peak with around 20% fewer counts. These fewer counts in the full photopeaks are also responsible for the continuum between the 1.332 MeV photopeak and the 2.505 MeV sum peak, as well as the sum peak itself having fewer counts in the GEANT4 model compared to the MCBEND and MCNP results.

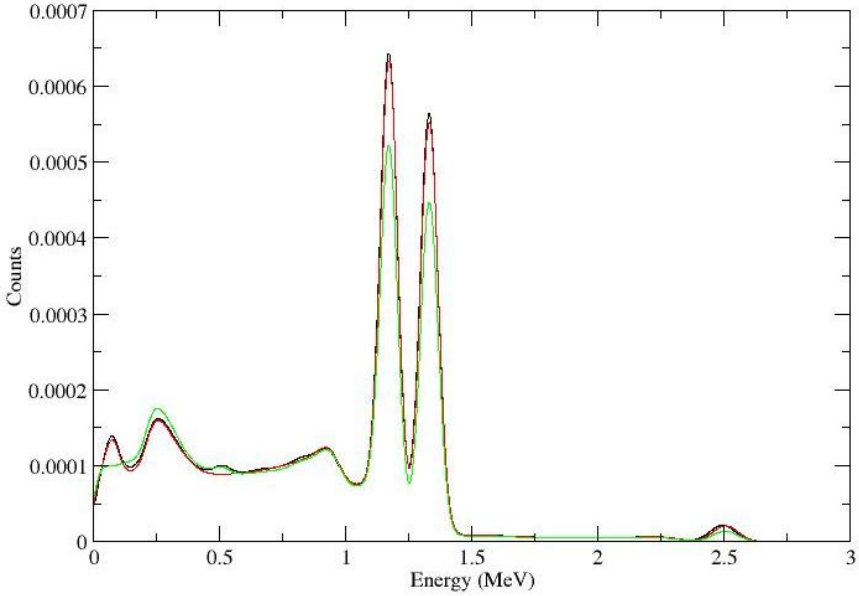

Figure 4.9 – Comparison of the three different Monte Carlo codes, MCBEND shown in black, MCNP shown in red and GEANT4 shown in green, for the response of a STEFF detector to ^{60}Co decay. The graph shows counts as a fraction of the 10 million sample batch size along the y axis on a linear scale as a function of energy in MeV along the x axis.

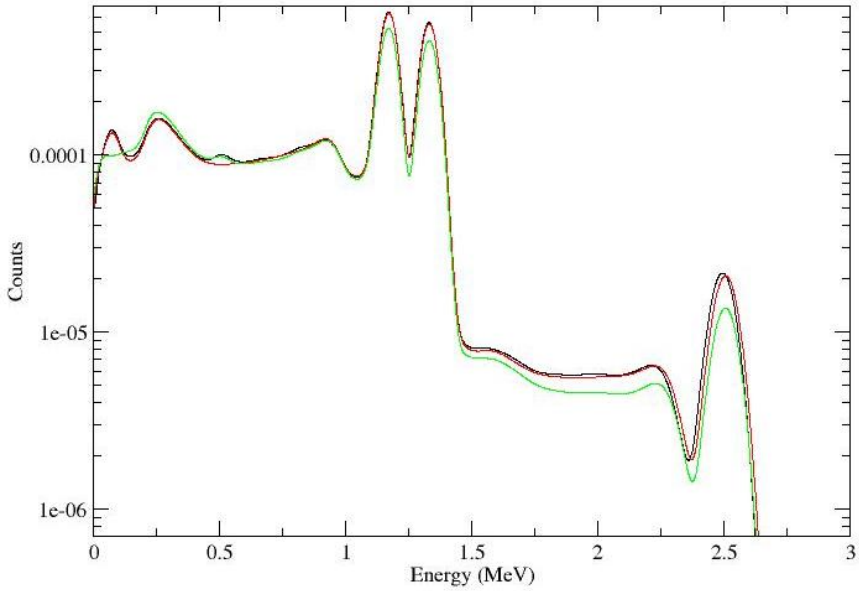

Figure 4.10 – Comparison of the three different Monte Carlo codes, MCBEND shown in black, MCNP shown in red and GEANT4 shown in green, for the response of a STEFF detector to ^{60}Co decay. The graph shows counts as a fraction of the 10 million sample batch size along the y axis on a logarithmic scale as a function of energy in MeV along the x axis.

Another noticeable difference is that the MCBEND and MCNP simulations have produced a peak at an energy lower than that of the backscatter peak. This is the codes attempt to produce the effect of fluorescent X-rays produced by gamma-ray interactions with the lead brick in the geometry. GEANT4 has made no such attempts to calculate the production of fluorescent X-rays in the lead.

However, GEANT4 does produce slightly more counts in the backscatter peak. MCBEND and MCNP overlap again almost identically.

The 511 keV pair production peak is evident in the spectra for MCBEND and GEANT4 however MCNP does not appear to have produced one. Under closer inspection of the raw data there is a very small peak in the MCNP model that is lost in the broadening of the data and pair production calculations do eventually produce more prominent features in the structure of the output spectra for MCNP at higher energies as can be seen in Figure 4.11, which shows single line spectra for the three codes for a 4 MeV photon. As with the previous graphs, results for MCBEND are shown in black, MCNP in red and GEANT4 in green.

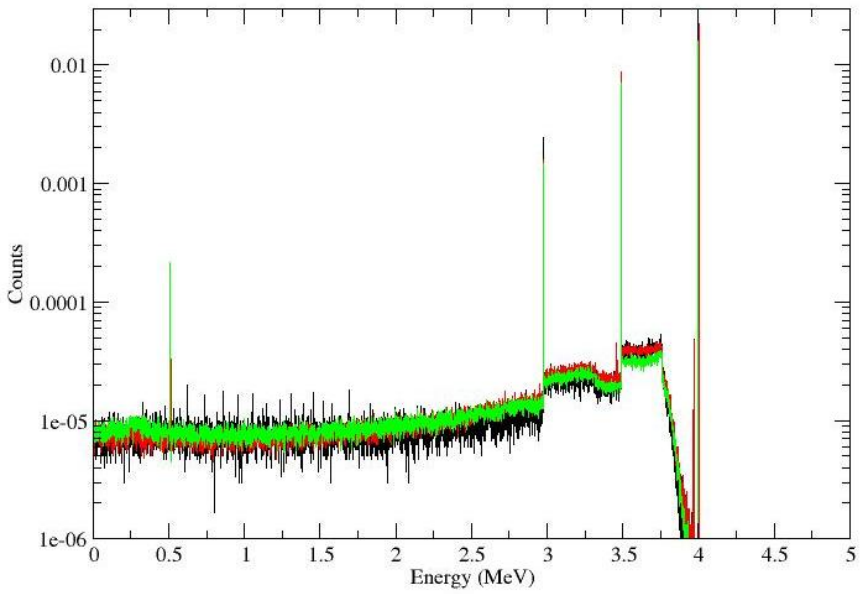

Figure 4.11 - Comparison of the three different Monte Carlo codes, MCBEND shown in black, MCNP shown in red and GEANT4 shown in green, for a gamma ray of energy 4 MeV. The graph shows counts as a fraction of the 10 million sample batch size along the y axis on a logarithmic scale as a function of energy in MeV along the x axis.

Figure 4.11 shows the single line spectra results for the three codes at a high photon energy of 4 MeV. Noticeable features include the 511 keV pair production annihilation peak as well as the 3489 keV single escape and 2978 keV double escape peaks. All three codes deal well with the single and double escape peaks, however only GEANT4 produces a significant peak for the 511 keV peak. MCNP again produces a very small peak and MCBEND produces several small peaks along the Compton continuum with no apparent physical explanation.

Under further investigation it appears this feature in MCBEND becomes much worse the higher the energy of the photon involved in the model is. Figures 4.12 and 4.13 show the line spectra produced for a 5 MeV and 6 MeV gamma-ray energy respectively.

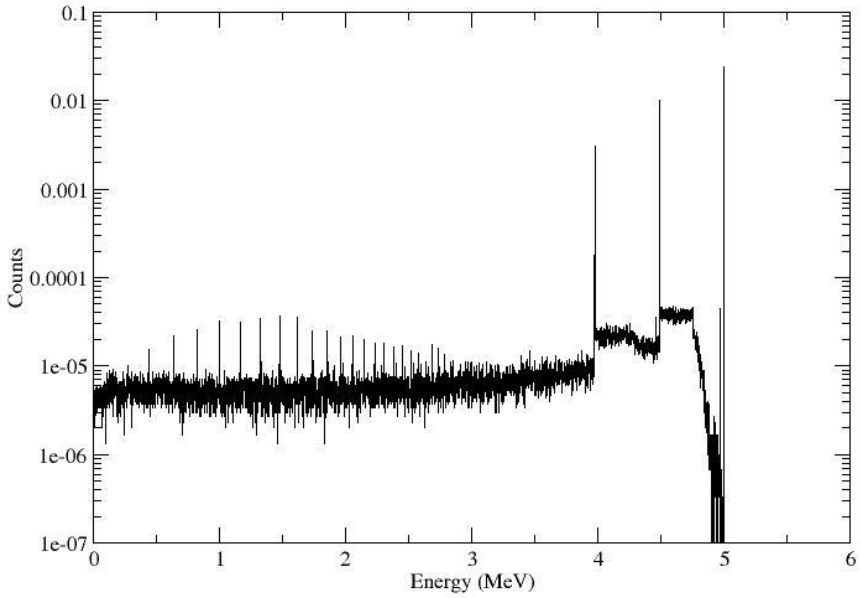

Figure 4.12 - Line spectrum for 5 MeV photon produced by MCBEND. The graph shows counts as a fraction of the 10 million sample batch size along the y axis on a logarithmic scale as a function of energy in MeV along the x axis.

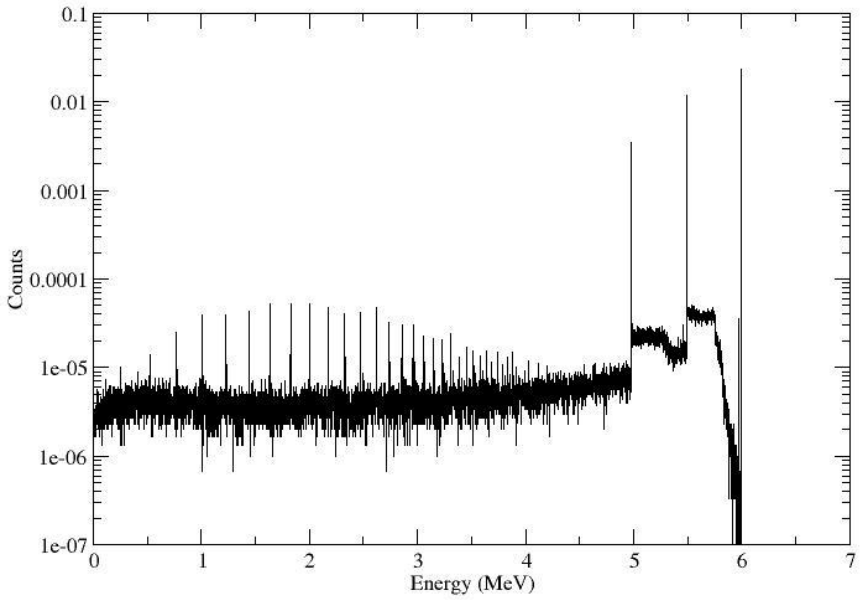

Figure 4.13 - Line spectrum for 5 MeV photon produced by MCBEND. The graph shows counts as a fraction of the 10 million sample batch size along the y axis on a logarithmic scale as a function of energy in MeV along the x axis.

The ANSWERS help desk was emailed to inquire as to what this feature was and the following reply was given:

> *"The spikes in the plots seem to be related to the condensed history method used in MCBEND for electron tracking. (It is also used in other codes.) In the MCBEND implementation, the condensed history method involves sampling for events at specific energies, and so there is a discrete nature to the process. The fineness of your scoring bins is picking this out. Probably the behaviour is also dependent on having pair production events, which happen at higher energies.*
>
> *The number of energy points used in the electron tracking can be adjusted via the STEP keyword in the ELECTRON DATA input. Increasing the NSTEP value from the default (12) to 20, reduced the effect, and increasing it further to a value of 100 seemed to eliminate it altogether."*

Comparisons of the three codes show that depending on the application in mind, no one program is better than the other. MCBEND produces a large amount of counts in both the 1.173 MeV and 1.332 MeV photopeaks which results in the production of an accurate sum peak. It can also deal well with pair production calculations at lower energies and produce prominent escape peaks for higher

energy photons, however at large energies it does produce some odd features. MCBEND can also produce peaks for fluorescent X-rays at low energies, an X-ray escape peak can also be observed next to the full photopeak, the single and double escape peaks.

MCNP also produces large numbers of counts in the photopeaks and so too produces accurate sum peaks. It can produce fluorescent X-ray peaks and X-ray escape peaks, as well as good single and double escape peaks, however it struggles to produce the 511 keV annihilation peak.

GEANT4 does not produce as large a number of counts in its photopeaks as MCBEND and MCNP and as a result a smaller sum peak height is calculated. It also does not calculate any X-ray fluorescence in the material in the model. It does however deal well with the production of the both the single and double escape peaks, as well as the 511 keV annihilation peak at all energies.

The vast majority of time spent on this project was taken up by waiting for simulations to run, because of this, it is worth making comparisons between the computing times of the three different codes, as well as the structures of the spectra produced.

The MCBEND program was run on RedQueen, the University of Manchester's high-performance computer cluster made up of over 800 cores with over 8GB of RAM each. The runs made for the models used in the section of the experiment took approximately 40 minutes, however, the geometry for these models were simplistic in their design. More complex models could take a matter of hours to run.

MCNP simulations were run on a laptop, with 2GB of RAM and a dual-core processor with 2.10 GHz of processing speed per core. Runs made would only utilize one of the processors core, this allowed for two simulations to be run at the same time on the same computer. This however was not necessary as runs for the simple geometries used in this part of the project generally took approximately 2 minutes to complete.

GEANT4 was also run on RedQueen. Runs for the geometries used to produce the above results took approximately 10 minutes.

Although the MCBEND and GEANT4 have significantly larger computing times than MCNP, they have the advantage of being run on RedQueen. RedQueen can be accessed remotely and lists of jobs queued with ease.

4.3 Production of the gamma-ray energy reference library and the structure of a ^{152}Eu spectrum

From the comparisons of the different modelling codes made in Section 4.2, MCBEND was chosen to be used in the production of the reference library. It was chosen because it modelled the experimental results well in Section 4.1 and for the range of energies used in the library, 50 keV to 1500 keV, produced good structures for the spectrum without any unusual features.

Firstly, the gap in energy of the photopeak was chosen by making several runs with photopeaks of different energies. A base gamma-ray energy of 800 keV was chosen to start with. Runs were then made for gamma-ray energies of 900 keV, 850 keV and 825 keV. The 800 keV energies were then scaled up by the scaling factor, *S*, given by Equation 14.

The results are shown for both unbroadened line spectra scaled to equal photopeak energies and spectra that are broadened and then scaled in Figures 4.14 to 4.19. The scaled spectra are shown in red and the unscaled in black.

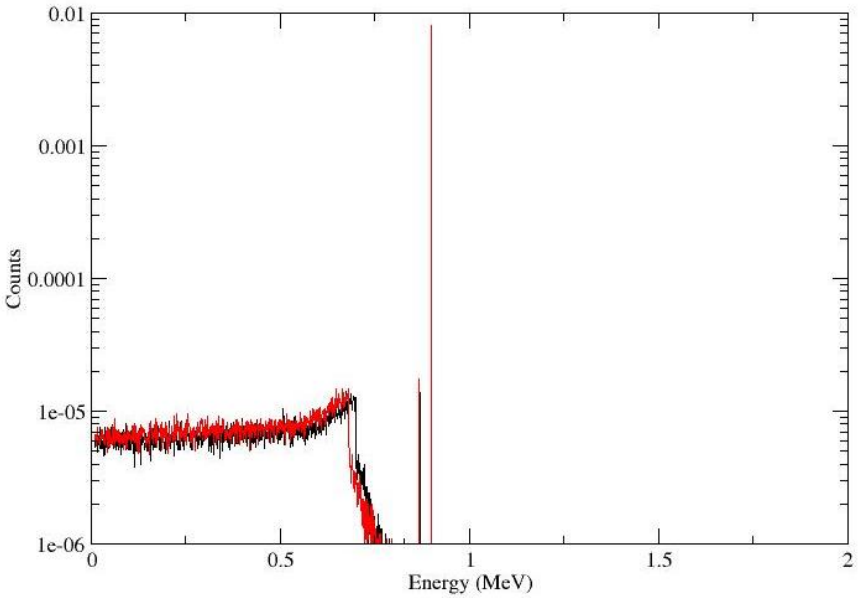

Figure 4.14 – Overlap of unbroadened line spectra for a 900 keV gamma-ray energy spectrum produced by MCBEND, shown in black and an 800 keV spectrum with energies scaled up to give a full photopeak at 900 keV, also produced by MCBEND and shown in red.

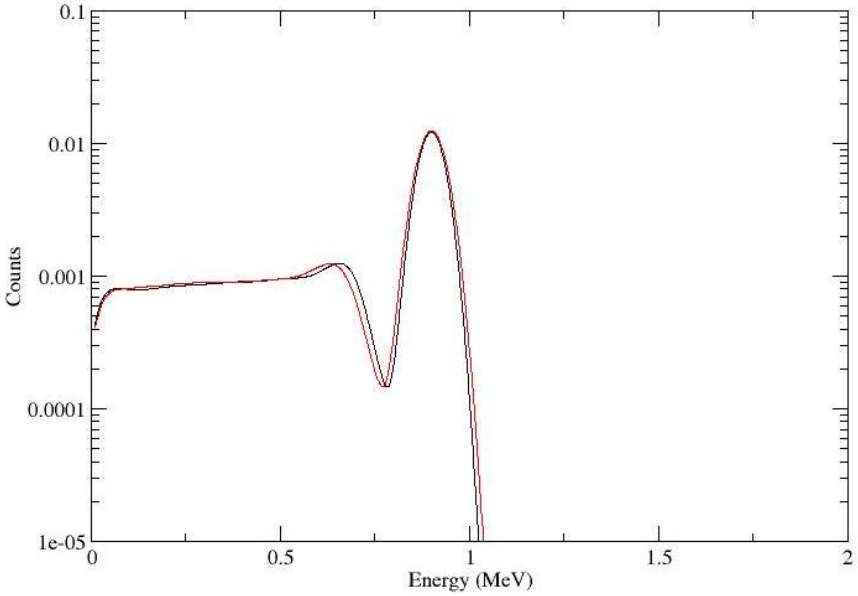

4.15 – Overlap of broadened spectra for a 900 keV gamma-ray energy spectrum produced by MCBEND, shown in black and an 800 keV spectrum broadened and subsequently energetically scaled to give a full photopeak at 900 keV, also produced by MCBEND and shown in red.

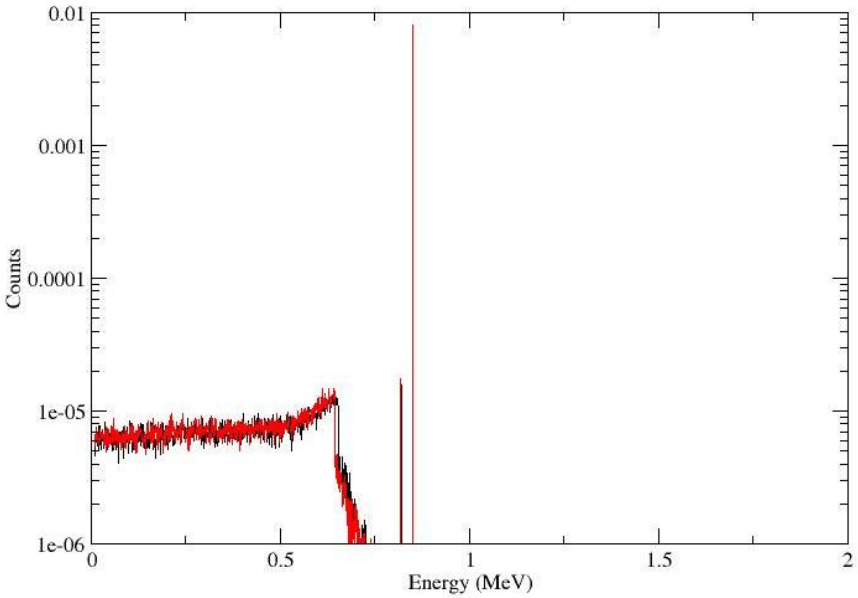

Figure 4.16 – Overlap of line spectra for a 850 keV gamma-ray energy spectrum produced by MCBEND, shown in black and an 800 keV spectrum with energies scaled up to give a full photopeak at 850 keV, also produced by MCBEND and shown in red.

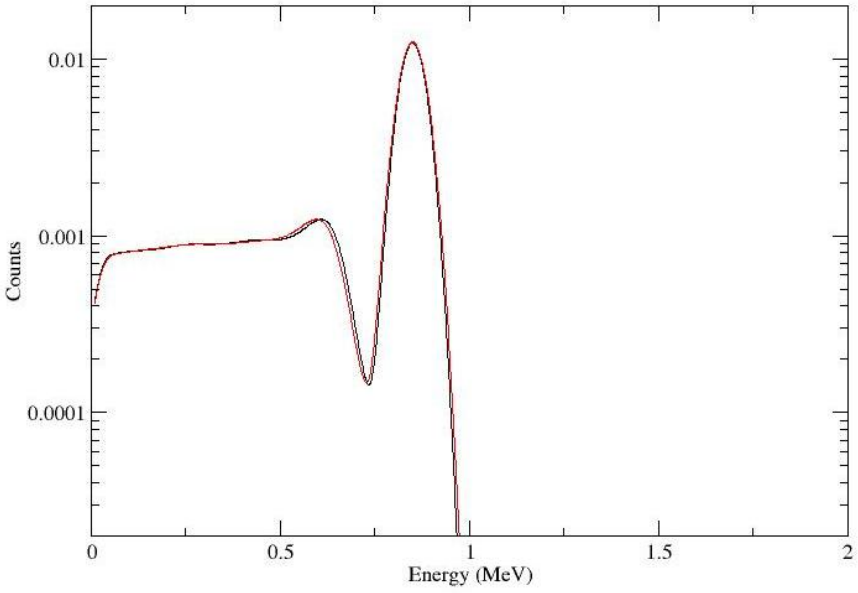

4.17 – Overlap of broadened spectra for a 850 keV gamma-ray energy spectrum produced by MCBEND, shown in black and an 800 keV spectrum broadened and subsequently energetically scaled to give a full photopeak at 850 keV, also produced by MCBEND and shown in red.

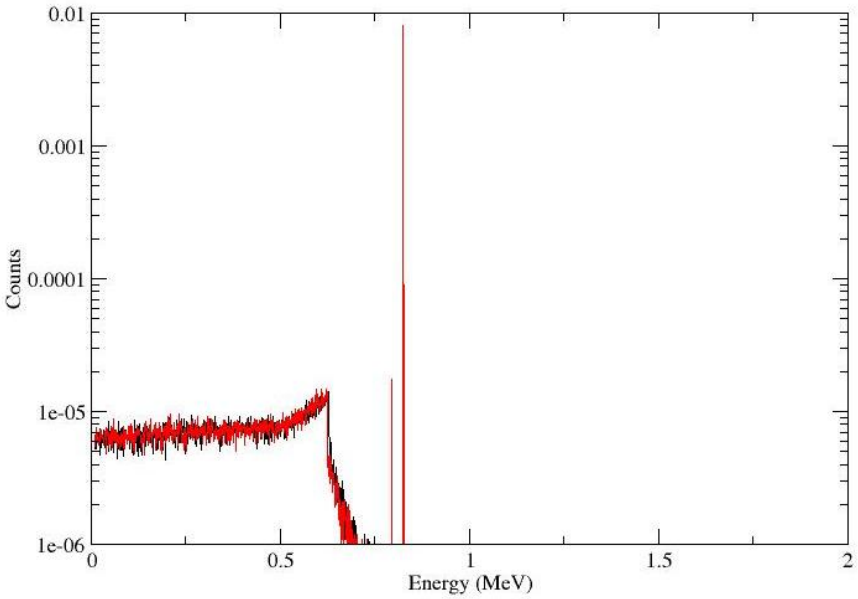

Figure 4.18 – Overlap of line spectra for a 825 keV gamma-ray energy spectrum produced by MCBEND, shown in black and an 800 keV spectrum with energies scaled up to give a full photopeak at 825 keV, also produced by MCBEND and shown in red.

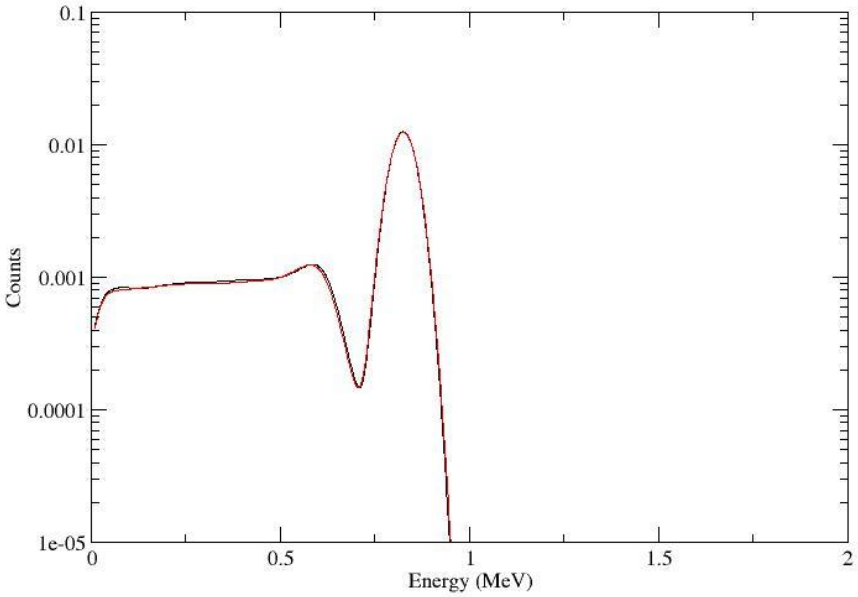

4.19 – Overlap of broadened spectra for a 825 keV gamma-ray energy spectrum produced by MCBEND, shown in black and an 800 keV spectrum broadened and subsequently energetically scaled to give a full photopeak at 825 keV, also produced by MCBEND and shown in red.

The results show improving overlap as the energy gap between the two spectra decreases, with a near perfect overlap observed in Figure 4.18 and Figure 4.19, the unbroadened and broadened spectra respectively, for a 25 keV gap between the scaled and unscaled spectra used. This means good results can be achieved by scaling reference spectra up or down by 25 keV and so, energy gaps between different photopeaks in the library can be made of size 50 keV.

Once the size of the energy gap was chosen, the library was produced by running simulations with single line gamma-ray energies ranging from 50 keV to 1500 keV in steps of 50 keV. The data was taken from the MCBEND output files and stored in .dat files with a two column format, the first column for energy and the second for the alpha value of each energy bin.

The spectra in the library were left unbroadened, in their single line structure. This was done so that appropriate broadening functions can be applied on the reference spectra that are specific to individual experimental spectra, for which the energy resolution may vary. The reference spectra were also normalised to the height of the full photopeak, this will make it easier to scale the heights of the spectra to appropriate gamma-ray intensities observed experimentally.

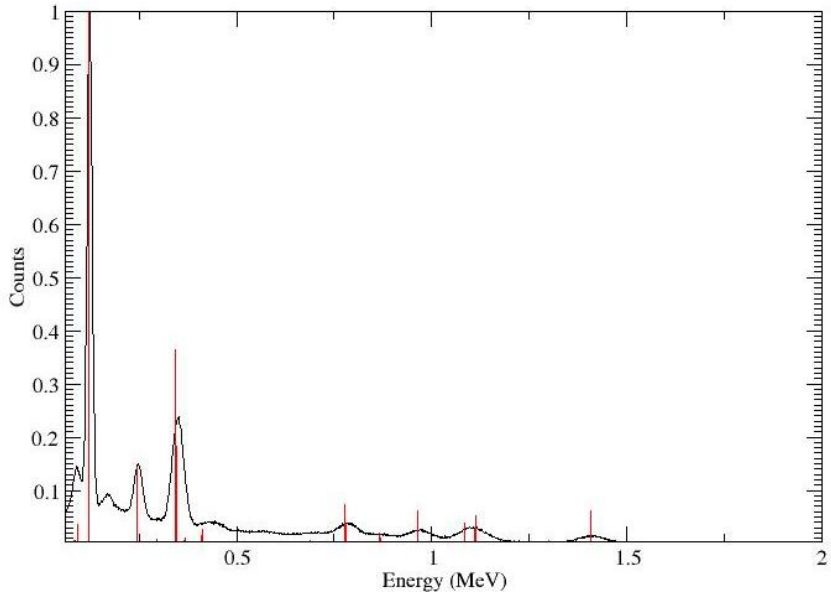

4.20 – ^{152}Eu decay spectrum taken by 51 mm by 51 mm NaI detector on the 20/03/2012 shown in black, the spectrum has undergone a background radiation subtraction. Line energy spectrum of ^{152}Eu decay produced by MCBEND shown in red. Counts are shown along the y axis on a linear scale, normalised to peak value as a function of energy in MeV along the x axis.

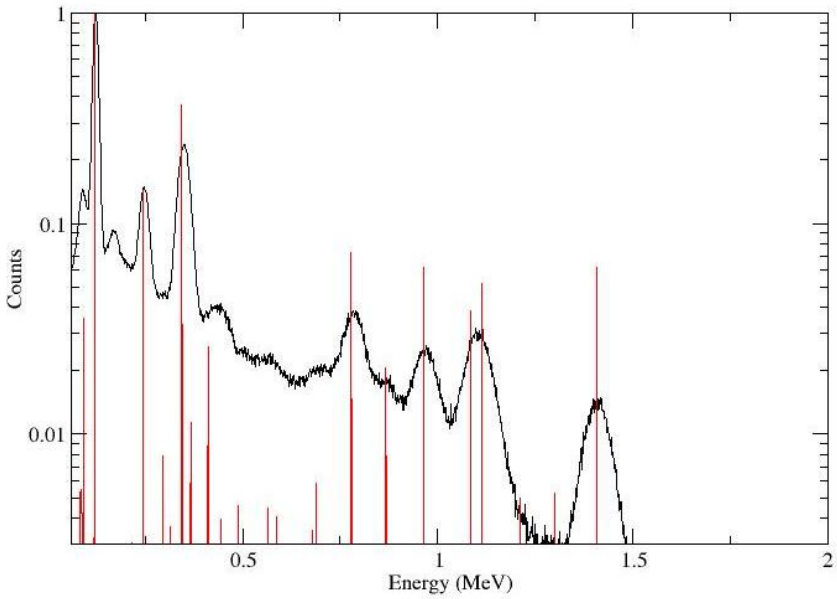

4.21 – ^{152}Eu decay spectrum taken by 51 mm by 51 mm NaI detector on the 20/03/2012 shown in black, the spectrum has undergone a background radiation subtraction. Line energy spectrum of ^{152}Eu decay produced by MCBEND shown in red. Counts are shown along the y axis on a logarithmic scale, normalised to the peak value as a function of energy in MeV along the x axis.

Figures 4.20 and 4.21 show results on a linear and logarithmic scale respectively, of experimental results taken for the decay of a ^{152}Eu source in black and MCBEND modelled line spectra. It is clear from the comparison between the observable peaks in experimentally taken results and those of the modelled results, whose energies and intensities are of known, identified gamma-rays produced in the decay of ^{152}Eu taken from [34], that many peaks produced with lower intensities are unobservable in the experimental results. This is due to the poor energy resolution of the NaI detectors used in experiment.

This effective loss of peaks will be a major problem for work done at STEFF, where experimentally measured spectra of nuclei with unknown decay schemes are taken. The problem cannot be addressed during the experimental stages of the work done in the STEFF project without replacing the detectors used in the apparatus with ones of better resolutions, however it could be solved during data analysis.

This could be done by identifying the clearly observable photopeaks along the spectrum, starting with that of the highest energy. A reference spectrum from the library would then be scaled to the appropriate height and energy, broadened according to the energy resolution of the results and then finally subtracted from the experimental data. This would remove the photopeak from the experimental results as well as any counts caused by Compton effects. The process would then be repeated for the photopeak with the next highest energy and so on in a step by step process. A sum-peak spectrum for all identified photopeak energies could then be constructed and subsequently stripped from the resulting spectrum.

This stripping of the spectrum using this method would eventually reveal any photopeaks that were previously hidden under counts in the experimental results, caused by the high intensity gamma-ray peaks. This method would in effect allow for the study of any previously unobservable photopeaks and in doing so, the structure of the nuclei being investigated.

One foreseeable problem with this method would be if there were two gamma-rays of similar energies. The peaks formed by these gamma-rays may produce what appears to be a single photopeak in the experimentally measured spectrum, which may be mistaken for a single gamma-ray energy during analysis of the spectrum. Care would have to be taken during stripping of a spectrum in case of such events.

5. Conclusion

The previous work has all been in aid of the furthering of the STEFF project. The work done, key among which is the production of the reference library, will be used in future experiments run by the STEFF project to further the present knowledge of nuclear structure.

The CoSpec program was successful in producing an accurate sum peak and can be further adapted in order to produce sum peak spectra for more than two photon energies. This will be useful for the analysis of nuclei with complex decays as it

will be possible to strip any sum peaks caused by sum events from any experimentally measured spectra, allowing for clearer observation of different gamma ray energies along a spectrum.

Another furthering of the work done here would be to create a computer program for stripping spectra. It would utilize the reference library and could even be combined with the Resbroad and CoSpec programs into one larger analysis program. It could work by inputting the energy resolution of the experimental results as a function of energy in order to produce appropriate broadening of the modelled results, peaks on the experimental data would then be identified and reference spectra in the library scaled appropriately and then broadened. A sum event spectrum could then be produced and then the identified peaks, as well as any calculated sum peaks stripped from the experimental results. The resulting spectrum would allow for observation of any peaks that were previously hidden under more prominent peaks and multiple sum events.

References

[1] Joseph Anthony Dare, *The Development of the Spectrometer for Exotic Fission Fragments*, School of Physics and Astronomy, Faculty of Engineering and Physical Sciences, University of Manchester, (2009).

[2] Private communications, A. J. Smith, Nuclear physics group, University of Manchester, (2012).

[3] Private communications, Scionix, (2012).

[4] Pedro Vaz, *Monte Carlo methods and techniques status and prospects for future evolution,* Applied Radiation and Isotopes, **68**, (2010) 536–541.

[5] *MCBEND - A Monte Carlo Program for General Radiation Transport Solutions – User Guide for Version 10,* issued by P. Cowan, (2007).

[6] J. K. Shultis & R. E. Faw, *An MCNP Primer,* Department of Mechanical Engineering, Kansas State University, (2011).

[7] William L. Dunn, J. Kenneth Shultis, *Monte Carlo methods for design and analysis of radiation detectors,* Radiation Physics and Chemistry, **78**, (2009), 852–858.

[8] P. Cowan, E. Shuttleworth, A. Bird & A. Cooper, *The Launch of MCBEND 10,* 10th International Conference on Radiation Shielding (ICRS-10) and 13th Topical Meeting on Radiation Protection and Shielding (RPS-2004), Funchal, Madeira Island, Portugal, (2004).

[9] B. L. Kirk, *Overview of Monte Carlo radiation transport codes,* Radiation Measurements, **45**, (2010), 1318-1322.

[10] N. R. Smith, E. Shuttleworth, S. J. Carter and M. Evans, *Geometry Modelling and Visualisation for the Monte Carlo Code MCBEND,* Proc. 8th International Conference on Radiation Shielding, (1994).

[11] J. Rowlands et al., *The JEF-2.2 Nuclear Data Library,* JEFF Report 17, OECD-NEA, (2000).

[12] M. Herman et al, *ENDF-6 Formats Manual,* National Nuclear Data Center, Brookhaven National Laboratory, (2005).

[13] T. Nakagawa, *Japanese Evaluated Nuclear Data Library Version 3 Revision-2: JENDL-3.2,* Journal of Nuclear Science and Technology, **32**, (1995), 1259-1271.

[14] P. Cowan, G. Dobson, G.A. Wright and A. Cooper, *Recent Developments to the Monte Carlo Code MCBEND*, 11th International Conference on Radiation Shielding (ICRS-11) and 14th Topical Meeting on Radiation Protection and Shielding (RPS-2008), Pine Mountain, Georgia, USA, (2008).

[15] G.A.Wright, E.Shuttleworth, M.J.Grimstone and A.J.Bird, *The Status of the General Radiation Transport Code MCBEND*, Proc. 5th Topical Meeting on Industrial Radiation and Radioisotope Measurement Applications, Bologna, Italy, (2002).

[16] J. F. Briesmeister, Ed, *MCNP – A General Monte Carlo N-Particle Transport Code, Version 4C,* LA-13709-M, (2000).

[17] Gregg C. Giesler, *MCNP software quality: then and now,* Proc. 10th International Conference on Software Quality, New Orleans, Louisiana, (2000).

[18] R. Kinsey, *Data Formats and Procedures for the Evaluated Nuclear Data File, ENDF*, Brookhaven National Laboratory report, 2nd Editions, (1979).

[19] R. J. Howerton et al., *The ILL Evaluated Nuclear Data Library (ENDL): Evaluation Techniques, Reaction Index, and Descriptions of Individual Reactions,* Lawrence Livermore National Laboratory report, **15**, Part A, (1975).

[20] M. A. Gardner and R. J. Howerton, *ACTL: Evaluated Neutron Activation Cross-Section Library - Evaluation Techniques and Reaction Index,* Lawrence Livermore National Laboratory report, Vol. 18, (1978).

[21] R. E. MacFarlane et al., *The NJOY Nuclear Data Processing System, Volume I: User's Manual*, Los Alamos National Laboratory report, Vol. I, (1982).

R. E. MacFarlane et al., *The NJOY Nuclear Data Processing System,*

Volume II: The NJO, RECONR, BROADR, HEATR and THERMR Modules, Los Alamos National Laboratory report, Vol. II, (1982).

[22] S. Agostinelli et al., *GEANT4 – a simulation toolkit*, Nuclear Instruments and Methods, **A** 506, (2003), 250-303.

[23] J. Allison et al., *GEANT4 Developments and Applications*, IEEE Transactions on Nuclear Science 53 No. 1 (2006) 270-278.

[24] GEANT4 Collaboration, *GEANT4 User's Guide for Application Developers*, (2011).

[25] GEANT4 Collaboration, *GEANT4 User's Guide for Toolkit Developers,* (2011).

[26] GEANT4 Collaboration, *Physics Reference Manual*, (2010).

[27] Glenn F. Knoll, *Radiation Detection and Measurement*, 2nd edition, John Wiley & Sons, Chichester, (1989).

[28] Kenneth S. Krane, *Introductory Nuclear Physics*, John Wiley & Sons, Chichester, (1988).

[29] John Lilley, *Nuclear Physics: Principles and Application*, John Wiley & Sons, Chichester, (2001).

[30] B. D. Milbrath et al., *Radiation detector materials: An overview*, Journal of Materials Research, **23**(10), (2008), 2561-2581.

[31] T. C. Billard & George Burns, *Time-delayed photoelectric effect*, Nature, **306**, (1983), 247-248.

[32] Arthur H. Compton, *A quantum theory of the scattering of X-rays by light elements*, Phys. Rev., **21**(5), (1923), 483-502.

[33] C. M. Davisson & R. D. Evans, *Gamma-Ray Absorption Coefficients*, Reviews of Modern Physics, **24**(2), (1952), 79-107.

[34] Richard B. Firestone, *Table of Isotopes: Eighth Edition Volume II*¸ 8th edition, John Wiley & Sons, Chichester, (1996).

Appendix A

Example of MCBEND input file.

```
!************************EXPERIMENTAL MODEL*****************************

BEGIN CONTROL DATA
SAMPLE LIMIT 100000000
END

BEGIN UNIFIED SOURCE DATA
GEOMETRY
POINT 0.0 0.0 0.0                !POINT SOURCE
ENERGY LINES 1.332               !1.332 MEV
SPECTRA 1                        !MONOENERGETIC
INTENSITY BODY 1
COMPONENT 1
END

BEGIN ENERGY DATA
GAMMA                                   !GAMMA-RAYS
SCORING GROUPS 596
FILL 1.5000 I 595*0.00250 P 0.0100      !TALLY RESULTS 0.01 TO 1.5 MEV, 1 KEV BINS
UNIFIED SOURCE
END

BEGIN ENERGY DEPOSITION
DETAILED PHD
SOME 1
END

BEGIN ELECTRON DATA
SHORT DATA LIST
MATERIALS 5
SOLID REACTION FULL
SOLID REACTION FULL
SOLID REACTION FULL
SOLID REACTION FULL
SOLID REACTION FULL
END

BEGIN MATERIAL GEOMETRY
@R1=[5.1/2]                     !CRYSTAL RADIUS AND DEPTH
@CD=5.1                         !CRYSTAL DEPTH
@OW=1                           !OPTICAL WINDOW THICKNESS
@AT=0.08                        !Al COATING THICKNESS
@DF=10                          !DETECTOR FRONT LENGTH
@ME=8                           !MOUNT EDGE LENGTH
@MT=2                           !MOUNT THICKNESS
@PMTL=15.5                      !PMT LENGTH
@EL=3                           !ELECTRONICS
@DL=[@DF+@MT+@PMTL+@AT]         !DETECTOR LENGTH
@SMSR=2                         !SOURCE MOUNT SMALL RADIUS
@MH=3                           !SOURCE MOUNT PLATE HEIGHT
@SMR=7.5                        !SOURCE MOUNT RADIUS
@SMH=6                          !SOURCE MOUNT HEIGHT
@BL=15.5                        !LEAD BRICK LENGTH
```

```
@BW=8                                   !LEAD BRICK WIDTH
@BD=5                                   !LEAD BRICK DEPTH

PART 1 NEST                             !CRYSTAL
XROD M1 0 0 0 @R1 @CD                   !NaI CRYSTAL

PART 2 OVERLAP                                                  !DETECTOR FRONT
XROD P1 @AT 0 0 @R1 @CD                                         !CRYSTAL
XROD M4 [@AT+@CD] 0 0 @R1 @OW                                   !OPTICAL WINDOW
XROD M0 [@AT+@CD+@OW] 0 0 @R1 [@DF-@CD-@OW-@AT]!HOLLOW
XROD M3 0 0 0 [@R1+@AT] @DF                                     !Al CASING

PART 3 OVERLAP                                                  !Al DETECTOR MOUNT
XROD M0 0 0 0 @R1 @MT                                           !HOLLOW
BOX M3 OXB 0 0 0 @MT @ME @ME                                    !Al DETECTOR MOUNT

PART 4 OVERLAP                                  !PM TUBE
XROD M2 [@PMTL-@EL-@AT] 0 0 @R1 @EL             !ELECTRONICS
XROD M0 0 0 0 @R1 @PMTL                         !HOLLOW
XROD M3 0 0 0 [@R1+@AT] [@PMTL+@AT]             !Al CASING

PART 5 CLUSTER                                  !DETECTOR
XROD P2 0 0 0 [@R1+@AT] @DF                     !DETECTOR FRONT
BOX P3 OXB @DF 0 0 @MT @ME @ME                  !Al MOUNT
XROD P4 [@DF+@MT] 0 0 [@R1+@AT] [@PMTL+@AT] !PM TUBE
BOX M0 OXB 0 0 0 @DL @ME @ME                    !WORLD

!PART 6 NEST                                    !Pb BRICK
!BOX M5 OXB 0 0 0 @BD @BW @BL                   !Pb BRICK

!PART 7 OVERLAP                                 !SOURCE MOUNT
!ZROD M3 0 0 @MH @SMSR @MH                      !TOP PLATE
!ZROD M3 0 0 0 @SMR @MH                         !BOTTOM PLATE
!ZROD M0 0 0 0 @SMR @SMH                        !WORLD

!PART 8 CLUSTER                                 !LAB
!BOX P5 OXB 5 0 0 @DL @ME @ME                   !DETECTOR
!BOX P6 OXB [-@BD-0.5] 0 3.5 @BD @BW @BL        !Pb BRICK
!ZROD P7 0 0 [-4.5-@SMH] @SMR @SMH              !SOURCE MOUNT
!BOX M0 -7.5 -7.5 -10.5 46 15 22                !WORLD
END

BEGIN MATERIAL SPECIFICATION
TYPE GAMMA
NORMALISE
ATOMS
MATERIAL 1 DENSITY 3.67 NA 1.0 I 1.0            !M1=NAI
MATERIAL 2 DENSITY 7.874 FE 1.0                 !M5=FE
WEIGHT
MATERIAL 3 ALUMINIUM                            !M2=AL
MATERIAL 4 GLASS                                !M3=GLASS
MATERIAL 5 LEAD                                 !M4=PB
END
```

Appendix B

Example of MCNP input file.

```
MSc project - STEFF detector and Pb brick
C
C material densities
C NaI,1=-3.67    Al,2=-2.70     Pb,3=-11.34
C
C            ############################           Define            Cells
################################
C
1 1 -3.67 -1 3 -4             imp:p 1   $NaI crystal
2 2 -2.70 -2 5 -6 #(-1 3 -4)  imp:p 1   $Al coating
3 3 -11.34 7 -8 9 -10 11 -12  imp:p 1   $Pb brick
4 0 -13 #1 #2 #3              imp:p 1   $define world
5 0 13                        imp:p 0   $define world

C
C           ############################          Define           Surfaces
##############################
C
1 cx 6.35                   $NaI crystal
2 cx 6.45                   $Al coating
3 px 5.08                   $crystal front
4 px 15.28                  $crystal back
5 px 5.00                   $detector front
6 px 15.38                  $detector back
7 px -5.5                   $Pb brick back
8 px -0.5                   $Pb brick front
9 py -4.0                   $Pb brick side
10 py 4.0                   $Pb brick side
11 pz -7.75                 $Pb brick bottom
12 pz 7.75                  $Pb brick top
13 so 25                    $world

mode p                      $photon trasnport
C
C ########################## Define Source ##############################
C 4 MeV gamma-ray emission source. Point source. Isotropic. At origin.
sdef pos=0 0 0 erg=d1
si1 l 0 4000e-3
sp1 d 0 1
C
C ######################### Define Tallies ############################
C
f18:P 1
e18 0 3999I 4.0             $tally energies 0 to 4 MeV in 1 keV bin size
C
C ######################## Define Materials ############################
C
m1 11000 0.5 53000 0.5                  $NaI
m2 13027 1                              $Al
m3 82000 1                              $Pb
C
C ######################## Define Run Time ############################
C
nps 10000000
```

Appendix C

Resbroad source code

```
      PROGRAM resbroad
!
      IMPLICIT NONE
      CHARACTER*128 confile, inpfile, outfile
      REAL c1, c2, c3, ofwhm, sigma, p, osq2pi, osig
      REAL, DIMENSION(:,:), ALLOCATABLE:: a, b
      INTEGER:: i, j, n, ierr
!
! Read input/output filenames and FWHM coefficients
!
      PRINT*,"RESBROAD"
      PRINT*,"  PLEASE ENTER CONTROL FILE NAME: "
      READ*, confile
      OPEN(10,file=confile,status="old")
      READ(10,*) inpfile
      READ(10,*) outfile
      READ(10,*) c1,c2,c3
      CLOSE(10)
      PRINT*,"  DATA INPUT  FILE NAME: ",TRIM(inpfile)
      PRINT*,"  DATA OUTPUT FILE NAME: ",TRIM(outfile)
      OPEN(20,file=inpfile,status="old")
      OPEN(30,file=outfile,status="unknown")
!
! Find length of spectrum then read in
!
      n=0
      DO
        ierr=0
        READ(20,fmt=*,iostat=ierr)
        IF(ierr/=0)EXIT
        n=n+1
      END DO
      ALLOCATE(a(4,n))
      ALLOCATE(b(n,n))
      a=0.0
      b=0.0
      REWIND(20)
      DO i=1,n
        ierr=0
        READ(20,fmt=*,iostat=ierr)a(1,i),a(2,i)
        IF(ierr/=0)PRINT*,"INPUT READ ERROR, LINE",i
      END DO
      CLOSE(20)
!
! Calculate energy-dependent sigmas
!
! ofwhm=1.0/(2.0*sqrt(2.0*log(2.0)))
      ofwhm=0.4246609
      IF(c3/=0.0)THEN
        DO i=1,n
          a(3,i)=c1+c2*sqrt(a(1,i)+c3*a(1,i)*a(1,i))
          a(3,i)=a(3,i)*ofwhm
        END DO
      ELSEIF(c2/=0.0)THEN
        DO i=1,n
          a(3,i)=c1+c2*sqrt(a(1,i))
          a(3,i)=a(3,i)*ofwhm
        END DO
      END IF
!
! Calculate Gaussian distribution
```

```
!
! osq2pi=1.0/sqrt(2.0*3.1415926)
      osq2pi=0.39894228*0.001
      osig=1.0/(c1*ofwhm)
      DO i=1,n
        IF((c2/=0.0).OR.(c3/=0.0))osig=1.0/a(3,i)
        DO j=1,n
          b(i,j)=osq2pi*osig*exp(-0.5*osig*osig*((a(1,j)-
a(1,i))**2))
          IF(b(i,j)<1E-6)b(i,j)=0.0
        END DO
      END DO
!
      DO i=1,n
        DO j=1,n
          a(4,j)=a(4,j)+a(2,i)*b(i,j)
        END DO
      END DO
!
! Ouput original and broadened spectra
!
      WRITE(30,"(A)")"  ENERGY      ORIGINAL    BROADENED "
      WRITE(30,"(3ES12.4)")(a(1,i),a(2,i),a(4,i),i=1,n)
      CLOSE(30)
      PRINT*,"  DONE! - GOODBYE!!!"
!
      END PROGRAM
```

Appendix D

CoSpec source code

```
//
// CoSpec
// CoSpec.cpp
// Program to produce coincidence event spectrum.
//


#include <iostream>           //allows program to perform input
and output
#include <fstream>            //allows   program   to   read   input
files and produce output files
#include <string>       //for strings
#include <sstream>            //move thigs from strings etc
#include <cmath>


using namespace std;

int main()     //begin program
{
      //variable declarations
      int ns;     //number of spectra used
      int nc;     //number of channels used

      string filename;
      stringstream stream;

      cout << "How many spectra used?" << endl;
//prompt   user   for   how   many   spectra   used   in   coincidence
calculation
      cin >> ns;                //read number of spectra

      cout << "How many channels per spectra?" << endl;
//prompt user for how many channels displayed in each spectrum
      cin >> nc;                //read number of channels

      //dynamic memory--DELETE!!!!!
      //make arrays for all the channels
      double ** arrayss = new double*[ns];

      for (int Ns = 0; Ns<ns; Ns++)
      {
            cout  <<  "Input  filename  for  spectrum"  <<  Ns+1  <<
endl;       //prompt user for input filenames
            cin >> filename;              //read input filename


            int m = (int)filename.size();
            char * infile = new char[m];

            stream << filename;
            stream >> infile;
            filename ="";
            stream.clear();

            //check file has opened
            ifstream workingfile ( infile );

            if(!workingfile.good())
            {
```

```
                  cerr << "Incorrect input file" << infile <<
endl;
                  exit(1);
            }


            //dynamic memory--DELETE!!!!!
            double * bobby;
            bobby = new double [nc];

            for (int j=0; j<nc; j++) {
                  workingfile >> bobby[j];

            }
            arrayss[Ns] = bobby;
            delete infile;

      }

      cout << "Output filename" << endl;        //prompt user for
output filename
      cin >> filename;                     //read output filename


      //make and open output file
      int m = (int)filename.size();
      char * outfile = new char[m];
      stream << filename;
      stream >> outfile;
      filename ="";
      stream.clear();
      ofstream outworkfile (outfile);
      delete outfile;


      //store and work on the output
      double outputarray[ns*nc];

      for (int i=0; i< ns*nc; i++)  outputarray[i]=0;

      //maths section
      for (int i=0; i<nc; i++) {
            for (int j=0; j<nc; j++) {
                  outputarray[i+j+ns-1]  +=  (((arrayss[0])[i]  )*(
(arrayss[1])[j]));
            }
      }


      cout << "testing maths:" << endl;
      for(int i=0; i<nc*ns ; i++){
            cout << "output " << i+1 << ":\t\t" << outputarray[i]
<< endl;
            outworkfile << outputarray[i] << endl;
      }

      //deleteing dynamic memory
      for (int i = 0; i < ns; i++)  delete[] arrayss[i];
    delete[] arrayss;

}
```